Title

An activity-regulated transcriptional program directly drives synaptogenesis.

Permalink

https://escholarship.org/uc/item/02z175xp

Journal

Nature Neuroscience, 27(9)

Authors

Yee, Callista
Xiao, Yutong
Chen, Hongwen
et al.

Publication Date

2024-09-01

DOI

10.1038/s41593-024-01728-x

Copyright Information

Peer reviewed

An activity-regulated transcriptional program directly drives synaptogenesis

Check for updates

Callista Yee [1], **Yutong Xiao**[2,8], **Hongwen Chen** [1,9], **Anay R. Reddy**[1], **Bing Xu**[3,4], **Taylor N. Medwig-Kinney**[2,10], **Wan Zhang**[2], **Alan P. Boyle** [5,6], **Wendy A. Herbst**[1], **Yang Kevin Xiang** [3,4], **David Q. Matus**[2] & **Kang Shen** [1,7] ✉

Although the molecular composition and architecture of synapses have been widely explored, much less is known about what genetic programs directly activate synaptic gene expression and how they are modulated. Here, using *Caenorhabditis elegans* dopaminergic neurons, we reveal that EGL-43/MECOM and FOS-1/FOS control an activity-dependent synaptogenesis program. Loss of either factor severely reduces presynaptic protein expression. Both factors bind directly to promoters of synaptic genes and act together with CUT homeobox transcription factors to activate transcription. *egl-43* and *fos-1* mutually promote each other's expression, and increasing the binding affinity of FOS-1 to the *egl-43* locus results in increased presynaptic protein expression and synaptic function. EGL-43 regulates the expression of multiple transcription factors, including activity-regulated factors and developmental factors that define multiple aspects of dopaminergic identity. Together, we describe a robust genetic program underlying activity-regulated synapse formation during development.

The molecular composition and architecture of synapses have been extensively characterized and are highly conserved in metazoans. The majority of synapses are formed in small temporal windows during development[1], suggesting the existence of a rapid and coordinated transcriptional program where cohorts of related genes are activated with precise control. These cohorts include pan-neuronally expressed genes, such as components of the synaptic vesicle cycle, and molecules that define specific neurotransmitter phenotypes. While neurotransmitter phenotype specification is known to be executed by terminal selector transcription factors (TFs)[2], less is known about the genetic programs regulating pan-neuronally expressed genes. In a recent study in *Caenorhabditis elegans*, CUT homeobox family TFs were shown to function redundantly to activate pan-neuronal genes[3], but how these

and other genetic programs are regulated to ensure functional connectivity between neurons remains elusive.

One mechanism that neurons may use to modulate hardwired genetic programs during synaptogenesis is through neuronal activity. Although it remains unclear if CUT TFs are regulated by activity, numerous studies have demonstrated that both spontaneous and sensory-driven activity function in synapse formation, synaptic plasticity and synaptic strength[4]. A large body of work pioneered in ref. 5 demonstrated that visual input and spontaneous activity have essential roles in the synaptic organization of the visual cortex during a critical period. During this period, active neurons establish more synaptic connections, while inactive neurons have fewer synapses and smaller axonal arbors. It is thought that synaptic transmission in input neurons

leads to depolarization and Ca^{2+} influx, which activates signal transduction pathways and ultimately results in activity-dependent transcriptional changes that impact synapse formation and plasticity[6,7]. The best-characterized TFs involved in this program are immediate-early genes (IEGs), such as *Fos* and *Jun*[8]. *Fos* has an important role in the development and function of the mammalian nervous system by acting as a strong transcriptional regulator[9]. Whether or how IEGs directly control synaptic gene expression is an important yet unanswered question.

Through a candidate approach using *C. elegans* dopaminergic neurons, we aimed to identify the mechanisms that drive activity-dependent synaptogenesis. Here we describe a new activity-regulated transcriptional program mediated by the conserved TFs EGL-43/MECOM and FOS-1/FOS. We demonstrate that both TFs bind directly to promoters of presynaptic genes, and loss of either factor reduces presynaptic gene expression. EGL-43 and FOS-1 mutually activate each other's transcription, and enhancing the binding of FOS-1 to the *egl-43* locus increases synaptic protein levels and subsequent synaptic transmission. In addition to activating presynaptic genes, EGL-43 modulates the expression of the terminal selector and CUT TFs, linking activity to hardwired genetic programs during development.

Results

Activity modulates synapse development in *C. elegans*

Although the role of activity in synapse development has been studied for decades, how activity regulates the expression of synaptic genes is unclear. To study these programs in vivo, we established the dopaminergic neurons of *C. elegans* as a model system. The posterior deirid (PDE) dopaminergic neurons possess bifurcating axons with numerous en passant synapses that can be visualized with endogenous, cell-type specific labeling of ELKS-1/ELKS, an active zone protein, using FLP/FRT-mediated recombination (FLP-on; Fig. 1a)[10,11]. We first tested if activity modulates presynaptic gene expression in PDE. To silence neurons, we expressed a histamine-gated chloride channel, HisCl1 (ref. 12), specifically in PDE. Silencing PDE during development led to a 22% decrease in ELKS-1 intensity along the length of the PDE axon (Fig. 1b–d). Animals lacking HisCl1 possess no defects in ELKS-1 intensity upon histamine treatment (Supplementary Fig. 1a,b). This finding contrasts with our previous work using overexpressed synaptic markers[13], highlighting the importance of endogenous labeling to detect sensitive changes in protein abundance.

We next asked if enhancing activity could increase presynaptic gene expression. We performed optogenetics using the blue light-gated sodium channel channelrhodopsin-2 (ChR2) to depolarize neurons[14]. We expressed ChR2 specifically in PDE and stimulated animals using blue light during axon outgrowth. Activation of ChR2 increased ELKS-1 intensity by 55% compared to controls (Fig. 1b,e,f and Supplementary Fig. 1c,d). Together, these results indicate that activity modulates synaptic gene expression in developing PDE neurons.

Given that transcription of *Fos* is highly induced by activity, we asked if *C. elegans fos-1* is similarly dependent. We endogenously tagged *fos-1*, the sole *Fos* ortholog, and found that silencing PDE decreased FOS-1 intensity by 31% (Fig. 1g,h) and excitation of PDE increased FOS-1 intensity by 25% (Fig. 1j–l). Normalization of FOS-1 intensity in PDEs to their sister posterior ventral neuron D (PVDs), which do not express transgenes, revealed similar changes in FOS-1 intensity (Fig. 1i,l). Notably, animals lacking either transgene exhibited no changes in FOS-1 intensity upon histamine or blue light treatment (Supplementary Fig. 1e,f). These results demonstrate that FOS-1 expression is regulated by activity, in agreement with studies in other systems[7]. Thus, PDE neurons are a suitable system to study the mechanisms of activity-regulated synaptic gene expression in vivo.

EGL-43/MECOM is expressed in the nervous system

Because activity-dependent TFs are involved in various cellular processes, we postulated that specific activation of synaptic genes might require interactions between activity-dependent TFs and specialized TFs to achieve specificity during development (Fig. 2a). To identify candidates, we searched for TFs that interact with activity-dependent TFs and whose orthologs are expressed in *C. elegans* neurons. We identified MECOM, a conserved TF known to activate the expression of *Fos*, *Jun* and *Egr1* and physically interacts with FOS, JUN and CREB[15].

In mammals, the *Mecom* locus encodes for three distinct TFs (PRDM3, EVI1 and MDS1) that are implicated in diverse biological processes, including cell proliferation, invasion and differentiation[16–18]. Partial loss-of-function mutations of *Mecom* in mice lead to embryonic hypocellularity in the neuroectoderm and failure of peripheral nerve formation[19]. *egl-43*, the sole *C. elegans* ortholog, encodes a C2H2 zinc-finger (ZF) TF possessing six evolutionarily conserved ZF domains (Fig. 2b)[20]. EGL-43 has been primarily studied in non-neuronal tissues but has been implicated in the migration of various neurons[20–23]. Notably, *fos-1* is a key target of EGL-43 in anchor cell invasion[23,24].

To study the expression of EGL-43 in the nervous system, we generated an endogenous green fluorescent protein (GFP)-tagged allele of *egl-43*. EGL-43 is first detected during embryogenesis in sensory neuron precursor nuclei (Supplementary Fig. 2a) and remains nuclear localized in sensory neurons throughout and after development (Supplementary Fig. 2b,c). Notably, EGL-43 is expressed in all dopaminergic neurons, including PDE. To understand the temporal activation of EGL-43 in neuronal differentiation, we compared the expression of EGL-43 to the well-characterized pro-neuronal basic-helix–loop–helix TF, HLH-2/E/Daughterless, which is ubiquitously expressed in neuronal lineages[25]. We generated an endogenous mScarlet-tagged allele of *hlh-2* and simultaneously imaged HLH-2 and EGL-43 in L2 to follow the V5.paa lineage, which ultimately gives rise to PVD and PDE (Supplementary Fig. 3). HLH-2 is first detected in the V5 seam cell (neuronal precursor) and is continuously expressed during subsequent cell divisions that generate PVD and PDE. Shortly after each cell has conferred neuronal fate, HLH-2 expression disappears. In contrast, strong expression of EGL-43 is only found in postmitotic neurons and is maintained until death (Supplementary Fig. 2b). These results suggest that EGL-43 is expressed in nascent postmitotic neurons, likely after commitment to become a neuron.

Loss of EGL-43 affects presynaptic protein expression

Because *egl-43* is rapidly expressed during PDE development, we tested its requirement for synapse formation. Null alleles of *egl-43* exhibit lethality and animals die before PDE is born[22]. To circumvent this, we used the auxin-inducible degron (AID) system where proteins of interest are tagged with an AID* tag, allowing for temporally precise degradation. In the presence of the synthetic hormone auxin, an exogenously expressed F-box protein, TIR1, recognizes AID*-tagged proteins, leading to poly-ubiquitination and subsequent degradation by the proteasome[26]. We used a strain carrying endogenous *egl-43::TagRFP-T::AID* paired with a single-copy transgene expressing TIR1 ubiquitously[26].

Shortly after PDE birth, but before axon outgrowth, L2s were moved onto media containing either 0 mM or 4 mM auxin and treated until L4. Degradation of EGL-43 led to a striking decrease of both endogenous ELKS-1 and RAB-3 along the axon of PDE (Fig. 2d–g). The reduction of synaptic markers was more pronounced in the distal axon than in the proximal axon, possibly due to proximal synapses forming first with less time for degradation of EGL-43 to occur. With this protocol, we did not detect any growth defects, exemplified by the presence of sparse synaptic markers in distal axons (arrowheads in Fig. 2d,f) and the presence of microtubules throughout the axon. This observation suggests that certain aspects of neurodevelopment are independent of EGL-43. Notably, auxin treatment of animals lacking *egl-43::TagRFP-T::AID* did not possess defects in synaptic markers (Supplementary Fig. 4), indicating that our degradation protocol is specific.

EGL-43 binds a conserved DNA binding sequence

Having established that EGL-43 is critical for presynaptic protein expression in PDE, we next investigated how EGL-43 promotes synaptogenesis.
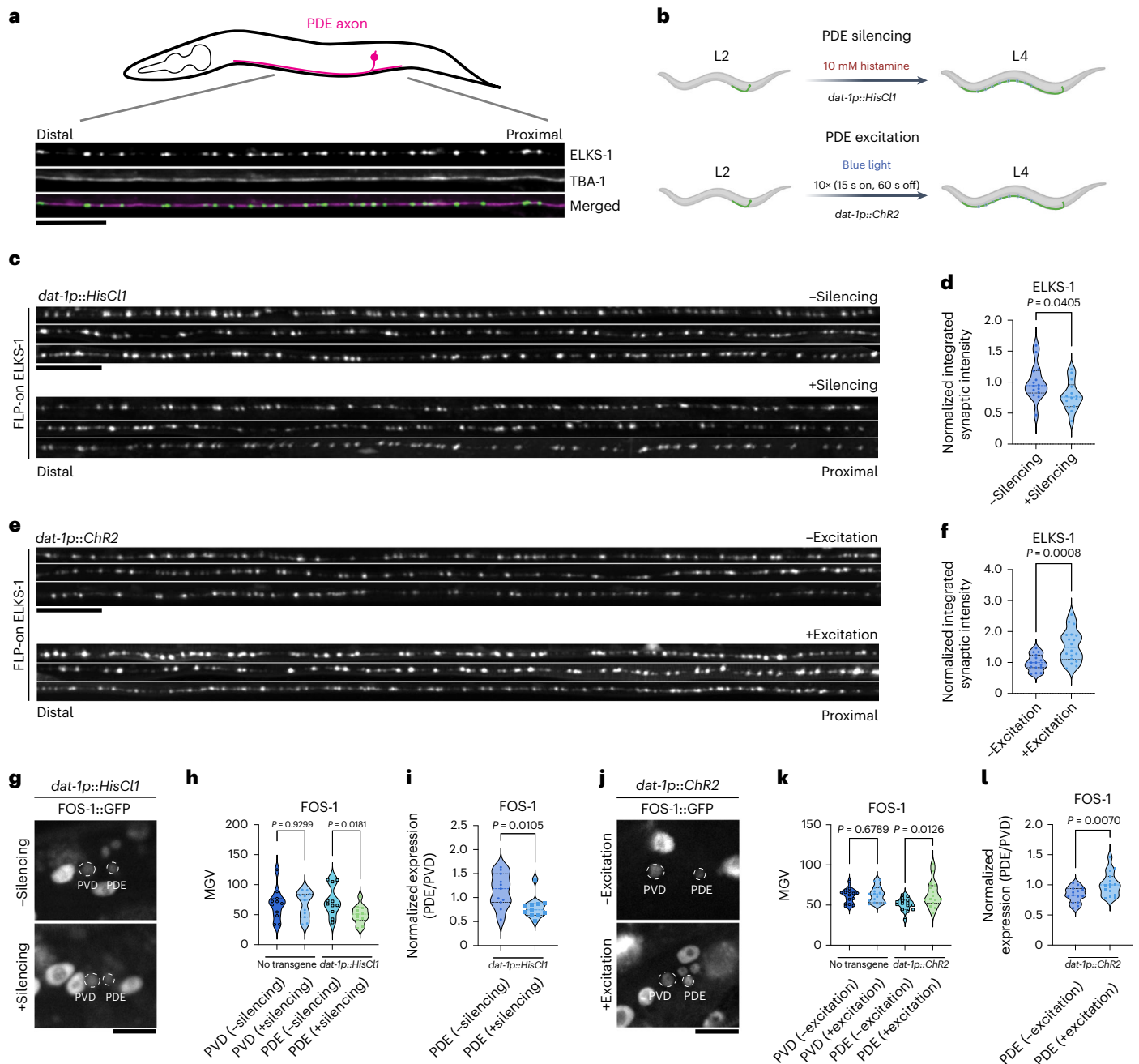
Fig. 1 | Neuronal activity modulates synapse formation in the developing PDE axon. a, Schematic representation and line scan of the PDE axon and its synapses labeled using a combinatorial approach. Endogenous FLP-on (FRT) GFP::ELKS-1 labels active zones and endogenous FLP-on (FRT3) mScarlet::TBA-1 labels microtubules (for axon morphology) when combined with a transgene expressing a dopaminergic-specific flippase (*dat-1p::FLP*). **b**, Top: schematic representation of PDE-silencing experiments. Transgenic animals expressing *dat-1p::HisCl1* were placed on media containing histamine at the L2 stage and imaged at the L4 stage. Bottom: schematic representation of PDE-excitation experiments. Transgenic animals expressing *dat-1p::ChR2* were subjected to blue light at the L2 or L4 stage and imaged either 2 h or 48 h post-treatment. This schematic was created with BioRender.com. **c**, Line scans of ELKS-1 in the PDE axon of animals carrying *wyEx8629(dat-1p::HisCl1)*, treated with 0 mM or 10 mM histamine. **d**, Quantification of ELKS-1 in PDE of animals shown in **c** (*n* = 14 for both conditions). **e**, Line scans of ELKS-1 in the PDE axon of animals carrying *wyEx10629(dat-1p::ChR2)*, treated with or without blue light. **f**, Quantification of ELKS-1 of animals shown in **e** (*n* = 19 for both conditions).

g, Transgenic animals carrying *wyEx8629(dat-1p::HisCl)* were imaged for their endogenous FOS-1::GFP signal in PVD and PDE neuronal nuclei (white dashed circles) in the presence or absence of 10 mM histamine. **h**, Quantification of FOS-1::GFP in animals shown in **f** (*n* = 11 for both conditions). **i**, Normalized expression of PDE FOS-1::GFP presented in **h**, compared to each paired PVD's (sister cell of PDE) expression (*n* = 11 for both conditions). **j**, Transgenic animals carrying *wyEx10630(dat-1p::ChR2)* were treated at L3 with or without blue light for ten cycles (15 s on and 60 s off) and allowed to recover for 2 h. FOS-1::GFP was imaged in PVD and PDE nuclei (white dashed circles). **k**, Quantification of FOS-1::GFP in animals shown in **i** (*n* = 15 for both conditions). **l**, Normalized expression of PDE FOS-1::GFP presented in **k** compared to each paired PVD's expression (*n* = 15 for both conditions). For images with line scans, scale bar = 20 μm; for images of neuronal nuclei, scale bar = 10 μm. For all graphs, medians are represented in thick dashed lines and quartiles are represented in thin dashed lines. *P* values presented were calculated using two-tailed unpaired Student's *t* tests. MGV, mean gray value.
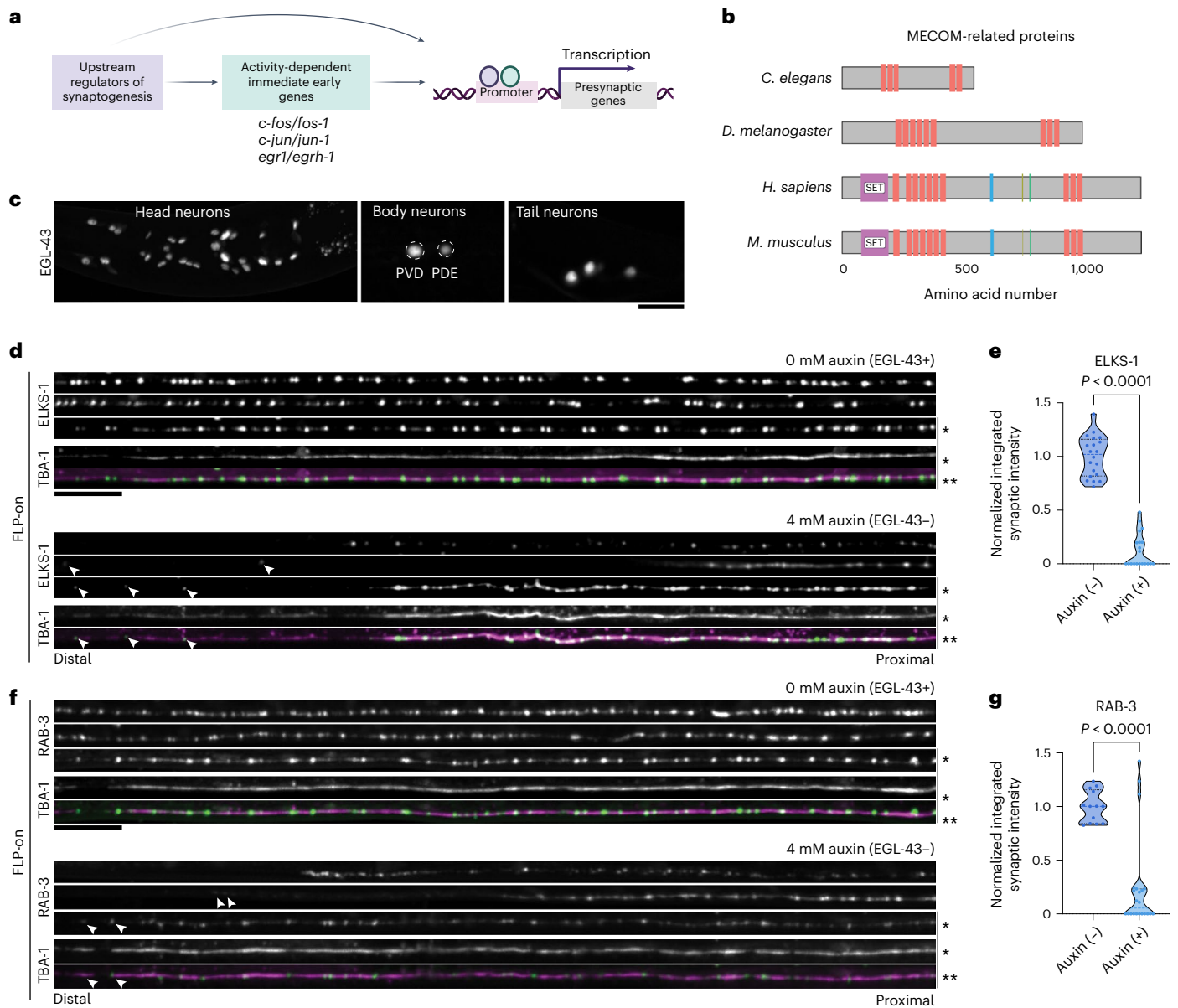
Fig. 2 | EGL-43 is expressed in sensory neurons and is critical for dopaminergic synaptogenesis. a, A potential model for activity-dependent synaptogenesis. Upstream, specialized TFs bind cooperatively with activity-dependent IEGs to activate downstream presynaptic targets. This schematic was created with BioRender.com. **b**, Comparison of MECOM-related proteins. From top to bottom: *C. elegans* EGL-43, *Drosophila melanogaster* Hamlet, *Homo sapiens* MECOM and *Mus musculus* MECOM. Features—red boxes represent ZF domains, purple boxes represent SET domains, blue boxes represent nuclear localization signal, gold boxes represent CTBP-binding motif 1 and green boxes represent CTBP-binding motif 2. **c**, Endogenous GFP-tagged EGL-43 is expressed in various sensory neuron nuclei, including head sensory neurons, the PVD and PDE neurons, and tail sensory neurons at the L4 stage ($n > 50$ animals examined, repeated thrice). **d**, Line scans of L4 PDE axons from *egl-43(wy1514)* animals expressing FLP-on ELKS-1 (to label active zones) and FLP-on TBA-1 (to label microtubules). Animals were treated with either 0 mM or 4 mM auxin. Line scans marked with single asterisk are imaged from the same worm to demonstrate the expression of both

labels in the same animal, with the final line scan of each set with both channels merged (denoted with two asterisks). White arrowheads denote ELKS-1 puncta detected in the distal axon. **e**, Quantification of line scan intensities of animals shown in **d** ($n = 20$ for both conditions). Medians are represented in thick dashed lines, and quartiles are represented in thin dashed lines; $P = 1.6215 \times 10^{-18}$. **f**, Line scans of L4 PDE axons from *egl-43(wy1514)* animals expressing FLP-on RAB-3 and FLP-on TBA-1. Animals were treated with either 0 mM or 4 mM auxin. Line scans marked with single asterisk are imaged from the same worm to demonstrate the expression of both labels in the same animal, with the final line scan of each set with both channels merged (denoted with two asterisks). White arrowheads denote weak RAB-3 puncta detected in the distal axon. **g**, Quantification of line scan intensities of animals shown in **f** ($n = 13$ (untreated) and $n = 22$ (treated)). Medians are represented in thick dashed lines and quartiles are represented in thin dashed lines; $P = 6.33578 \times 10^{-7}$. P values presented were calculated using two-tailed unpaired Student's t tests. Scale bar = 10 μm for all images.

We analyzed a whole-animal chromatin immunoprecipitation followed by sequencing (ChIP–seq) dataset of endogenous EGL-43 at L3 (ref. 24) and found a strong signal within 250 bp of transcription start sites (TSSs; Fig. 3a). EGL-43 binds numerous potential targets, but with minimal neuronal enrichment by Gene Ontology (GO) term analysis

(Supplementary Fig. 5 and Supplementary Table 6). However, EGL-43 is expressed in many non-neuronal cells, which may contribute to the lack of neuronal terms we observed.

Given the strong phenotype upon loss of EGL-43 in PDE, we investigated the targets of EGL-43 in dopaminergic neurons. We turned
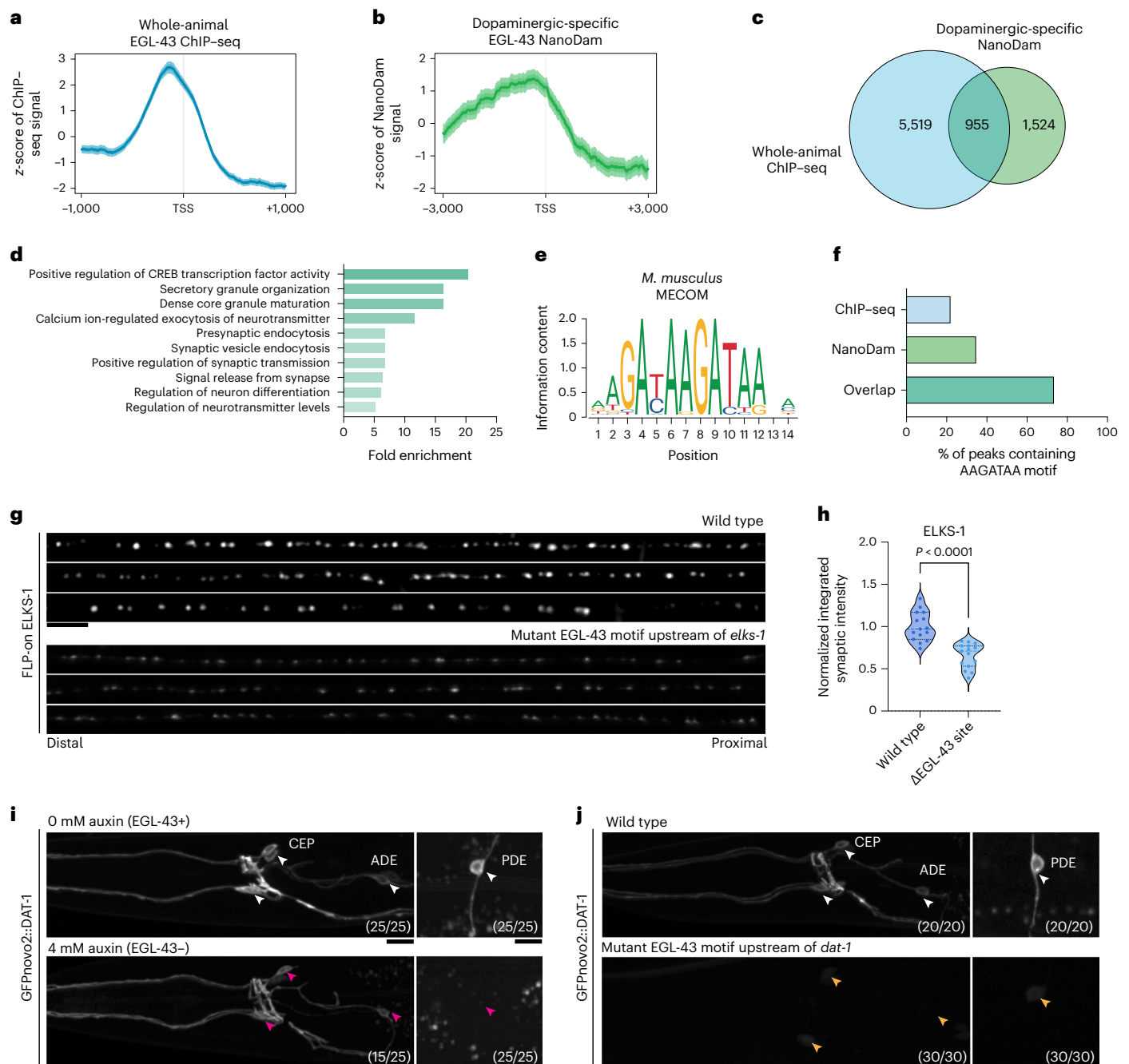
Fig. 3 | EGL-43 is a conserved ZF TF that controls presynaptic gene expression. a, Aggregation plot of EGL-43 ChIP–seq signal across *C. elegans* genes. **b**, Aggregation plot of EGL-43 dopaminergic-specific NanoDam signal across *C. elegans* genes. For **a** and **b**, bold lines represent the mean signal, darker shading represents the estimated s.e. and lighter shading represents the 95% confidence interval. **c**, Venn diagram comparing EGL-43 ChIP–seq and dopaminergic-specific NanoDam datasets. Numbers represent peaks, either overlapping or unique to each dataset. **d**, GO analysis performed on the overlapping peaks between ChIP–seq and NanoDam datasets (PANTHER biological process). **e**, JASPAR TF binding profile for mouse (*M. musculus*) MECOM. **f**, Proportion of peaks within EGL-43 profiling datasets that contain a 5′-AAGATAA-3′ motif. **g**, Line scans of three PDE axons in animals carrying FLP-on ELKS-1 in the wild type and *elks-1(wy1823)*, which possess a mutant EGL-43 motif. **h**, Quantification of PDE axon line scans of animals shown in **f**. $P = 2.50832 \times 10^{-6}$ and was calculated using a two-tailed

unpaired Student's *t* test. $n = 15$ for both genotypes. Medians are represented in thick dashed lines, and quartiles are represented in thin dashed lines. **i**, Representative micrographs of endogenous DAT-1 signal in animals carrying EGL-43::TagRFP-T::AID*. Animals were subjected to auxin treatment for 48 h. Arrowheads denote cell bodies of dopaminergic neurons (white, 0 mM auxin, and pink, 4 mM auxin). Numbers indicate the number of animals that resemble the phenotype shown in images. This experiment was repeated four times with similar penetrance. **j**, Representative micrographs of endogenous DAT-1 signal in wild-type animals and animals and *dat-1(wy1824)*, which possess a mutant EGL-43 motif. White and yellow arrowheads indicate dopaminergic neuron cell bodies of respective genotypes. Numbers indicate the number of animals that resemble the phenotype shown in images. This experiment was repeated thrice with similar penetrance. Scale bar = 10 μm for all images.

to tissue-specific genomics using NanoDam, a modified version of DamID[27]. Although NanoDam results in larger peaks and does not provide the same resolution as ChIP–seq, it enables the identification of targets on a tissue-specific basis[27]. Briefly, a Dam-methylase fused to a GFP-nanobody was driven using the *dat-1* promoter and inserted into the genome as a single-copy transgene. This transgene was then crossed into worms carrying endogenous EGL-43::GFP. The Dam-methylase nanobody fusion is recruited to genomic regions where EGL-43 is bound, leading to proximity-based labeling of DNA. We examined an EGL-43 NanoDam dataset that we have recently generated[28] and detected large peaks upstream of TSSs (Fig. 3b), complementing our observations by ChIP–seq. We observed a significant overlap between dopaminergic-specific NanoDam and whole-animal ChIP–seq (955/2,479 peaks, Fisher's exact test: $P = 2.8179 \times 10^{-158}$; Fig. 3c and Supplementary Tables 2 and 3). GO term analysis revealed strong enrichment for neuronally associated terms in the overlapping genes (Fig. 3d and Supplementary Tables 7 and 8). Combining the findings from both datasets, EGL-43 was bound to genes encoding many presynaptic proteins, including synaptic vesicle-associated proteins, such as the Rab GTPase *rab-3*/RAB3, and active zone proteins, such as *elks-1*/Elks, *cla-1*/Bassoon/Piccolo, *syd-2*/Liprin-α and *unc-10*/Rim.

Because EGL-43 binds to many genes encoding presynaptic proteins and loss of EGL-43 reduces presynaptic protein intensity, we wondered if EGL-43 directly activates presynaptic gene expression. Although the consensus binding motif of EGL-43 has never been characterized, its ZF domains are highly homologous (~80%) to those of MECOM[20]. The binding motif of the first four ZF domains of mouse MECOM has been well studied, with a consensus sequence of 5′-GA(C/T)AAGA(T/C)AAGATAA-3′ (ref. 29; Fig. 3e). We hypothesized that EGL-43 binds a similar sequence and examined our datasets for the core motif of 5′-AAGATAA-3′. We found that 22% of ChIP–seq peaks and 36% of NanoDam peaks contained this putative motif (Fig. 3f). However, of the overlapping peaks between the datasets, the motif was present in 73% (700/955) of the peaks, supporting our hypothesis that EGL-43 binds a conserved sequence.

We scanned the combined EGL-43 NanoDam and ChIP–seq peaks within the promoters of multiple presynaptic genes, including *elks-1* and the dopamine transporter *dat-1*, and found several putative motifs (5′-AAAAGATAG-3′ and 5′-AAAAGATAA-3′) that resemble the consensus sequence for MECOM. These motifs were present in regions of open chromatin, as identified through assay for transposase-accessible chromatin with sequencing (ATAC–seq) of neuronal nuclei, reinforcing the idea that EGL-43 might directly bind DNA to modulate gene expression (Supplementary Fig. 6a). To validate binding, we performed ChIP–quantitative polymerase chain reaction (qPCR) on endogenous EGL-43 using primer sets that span *elks-1*. We found increased binding of EGL-43 to an upstream region corresponding to a ChIP–seq peak containing a putative EGL-43 motif (Supplementary Fig. 6b).

We then tested if EGL-43 binding is necessary to modulate gene expression by mutating its putative binding sites. Using genome editing, we mutated the putative site (5′-AAAAGATAG-3′ to

5′-AACCCCCCC-3′) upstream of *elks-1* in animals carrying endogenously *FLP-on::GFP::elks-1*. This permutation was shown in vitro to abolish the binding of EVI1, a TF encoded by *Mecom*, to the phosphatase and tensin homolog locus[30]. Mutation of this sequence reduced *elks-1* transcript levels (Supplementary Fig. 7a), ultimately leading to reduced ELKS-1 intensity in PDE (Fig. 3g,h). Although this reduction in ELKS-1 is not as prominent as that observed upon degradation of EGL-43, it indicates that other factors, which may be controlled by EGL-43, contribute to *elks-1* expression.

Having found a critical role for EGL-43 in the expression of *elks-1*, a core synaptic protein, we next considered if EGL-43 was more broadly regulating presynaptic proteins. The synaptic function of dopaminergic neurons is also critically dependent on dopamine transporters. We endogenously tagged *dat-1*, the plasma membrane dopamine transporter and the ortholog of human DAT, which is continuously expressed in all dopaminergic neurons (cephalic (CEP), anterior deirid (ADE) and PDE (Fig. 3i)). Auxin-induced degradation of EGL-43 at L2 resulted in a completely undetectable GFPnovo2::DAT-1 signal in PDE (Fig. 3i) by L4. We then tested if abolishing the binding of EGL-43 to *dat-1* would similarly decrease DAT-1 expression. Using genome editing, we mutated the putative binding site (5′-AAAAGATAA-3′ to 5′-AACCCCCCC-3′) upstream of *dat-1* and observed a striking reduction of DAT-1, to the extent where GFP was only detected in the cell body (Fig. 3j). We performed quantitative PCR with reverse transcription and confirmed that this mutation reduced *dat-1* transcripts (Supplementary Fig. 7b), indicating that EGL-43 directly controls *dat-1* expression. Although our degradation experiments did not yield as strong reduction of DAT-1 in other neurons compared to PDE (Fig. 3i), this may be due to limited exposure to auxin as those neurons are born and express DAT-1 embryonically. Together, these data provide evidence that EGL-43 functions as a transcriptional activator by binding directly to presynaptic genes to promote expression.

FOS-1 is critical for dopaminergic presynaptic gene expression

Increasing evidence suggests that synapse formation is regulated by activity, possibly through activity-triggered TF activation[31]. Therefore, we considered if EGL-43 links activity and synapse formation by activating IEGs to modulate synaptic gene expression. Consistent with mammalian studies, EGL-43 activates multiple IEGs, including *fos-1*/Fos during the development of non-neuronal cells[23]. FOS-1 has been implicated in activity-dependent axonal regeneration but has not been thoroughly investigated for its role in neuronal development[32].

C. elegans FOS-1 is normally expressed constitutively in all cells, including PVD and PDE (Fig. 4a). To understand the relationship between FOS-1 and EGL-43, we generated animals carrying both endogenous FOS-1::GFP and EGL-43::TagRFP-T::AID*. Auxin-induced degradation of EGL-43 decreased FOS-1 intensity in both PVD and PDE (Fig. 4a,b). Auxin treatment did not affect the expression of FOS-1 in animals lacking EGL-43::TagRFP-T::AID* (Supplementary Fig. 8a). These results indicate that FOS-1 expression is partially dependent on

Fig. 4 | FOS-1 is critical for presynaptic gene expression in dopaminergic neurons. a, Images of L4 animals carrying endogenous FOS-1::GFP and EGL-43::TagRFP-T::AID* treated with 0 mM or 4 mM auxin for 48 h. PVD and PDE neuronal nuclei are outlined (white dashed circles). Auxin experiments were repeated independently with similar results (*n* = 3). **b**, Quantification of FOS-1::GFP intensity of nuclei (*n* = 15 for both conditions). **c**, Venn diagram displaying overlap of peaks between dopaminergic FOS-1 NanoDam and EGL-43 NanoDam. **d**, Left: GO term analysis of genes mapping to FOS-1 NanoDam peaks. Right: GO term analysis of genes mapping to the overlap between FOS-1 and EGL-43 NanoDam peaks. **e**, Line scans of FLP-on GFP ELKS-1 in PDE axons. The top two sets of line scans correspond to animals carrying endogenous FOS-1::TagRFP-T::AID* that were treated with either 0 mM or 4 mM auxin. Images were thresholded in the same fashion. The line scan denoted with single asterisk
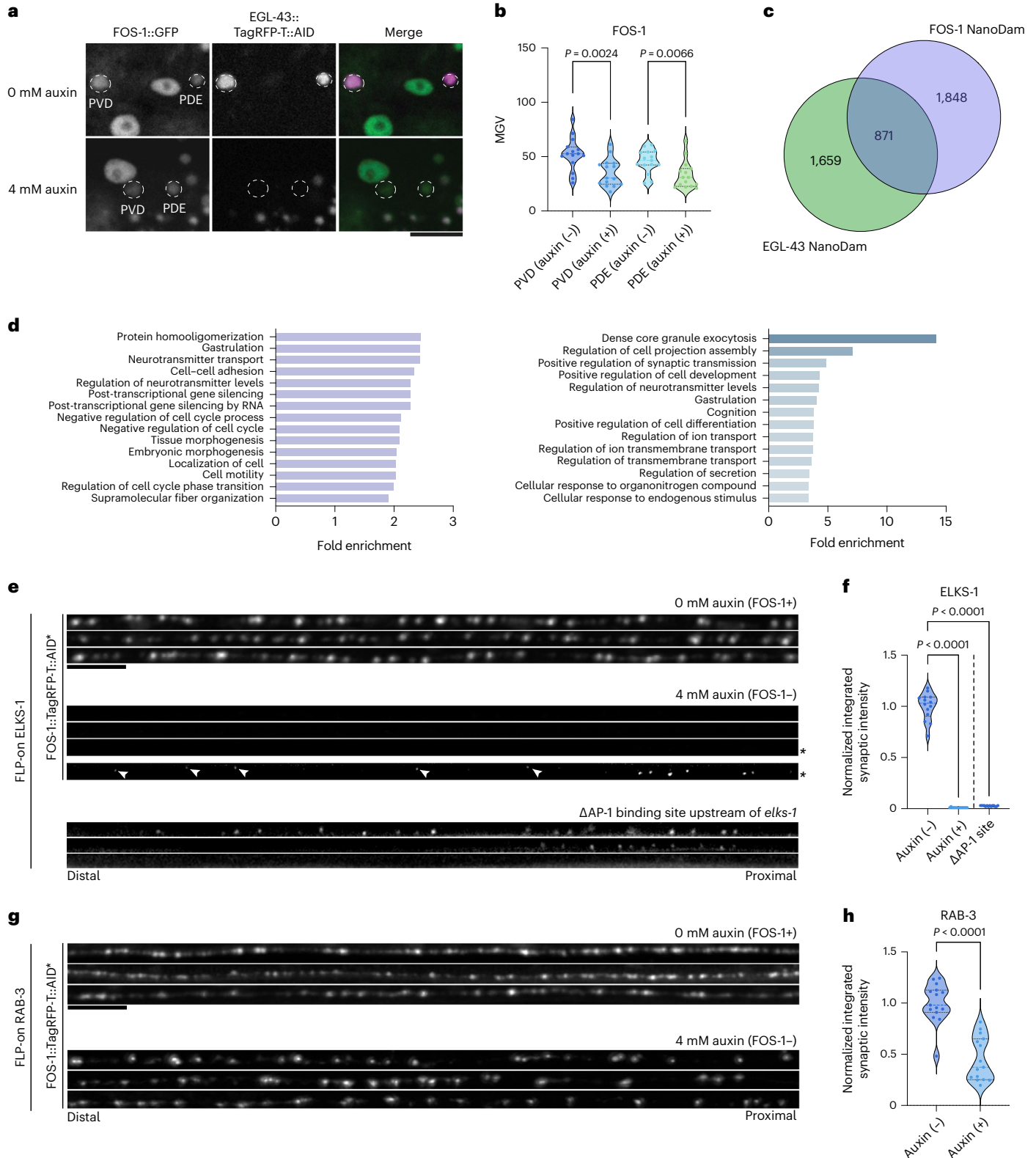
was thresholded to increase the visibility of synapses for illustrative purposes. Arrowheads point to small synapses that are nearly undetectable in the distal axon. The final set of PDE line scans corresponds to FLP-on ELKS-1 expression in animals with the AP-1 site deleted upstream of the TSS of *elks-1*. **f**, Quantification of line scans in **e**, where *n* = 14 for all conditions. For graph comparisons, $P = 5.77664 \times 10^{-21}$ for auxin (−) versus auxin (+) and $P = 8.76057 \times 10^{-21}$ for auxin (−) versus ΔAP-1 site. **g**, Line scans of FLP-on GFP RAB-3 in PDE axons of animals carrying FOS-1::TagRFP-T::AID*, treated with 0 mM or 4 mM auxin. **h**, Quantification of animals **i** (*n* = 15 for both conditions, $P = 5.21856 \times 10^{-8}$). For all graphs, medians are represented in thick dashed lines, and quartiles are represented in thin dashed lines. *P* values were calculated using two-tailed unpaired Student's *t* tests. Scale bar = 10 μm for all images.

EGL-43, further supported by the presence of EGL-43 ChIP–seq peaks at the *fos-1* locus (Supplementary Table 1).

To assess if EGL-43 is acting specifically or broadly affecting the expression of nuclear proteins, we tested the requirement of EGL-43 on endogenous SWSN-4 expression. *swsn-4*/*Brg1* encodes a subunit of the SWI/SNF chromatin remodeling complex and is expressed broadly, similar to *fos-1*. The *swsn-4* locus lacks EGL-43 ChIP–seq peaks, unlike

fos-1, and degradation of EGL-43 did not affect SWSN-4::GFP (Supplementary Fig. 8). Thus, it is likely that EGL-43 controls a discrete genetic program as opposed to causing global changes in transcription.

Next, we wondered if FOS-1 modulates the expression of similar genes as EGL-43. FOS-1 NanoDam peaks were associated with a functionally diverse set of targets with no apparent neuronal enrichment (Fig. 4c,d and Supplementary Table 9). However, when we compared

Fig. 4 | (a–h) FOS-1 analysis showing imaging of FOS-1::GFP and EGL-43::TagRFP-T::AID, quantification, NanoDam target overlap, gene ontology enrichment, and FLP-on ELKS-1 and RAB-3 synaptic intensity analyses.

FOS-1 NanoDam to EGL-43 NanoDam, we found significant overlap (871/2,719 FOS-1 peaks; Fisher's exact test, $P = 3.2653 \times 10^{-298}$), with enrichment of neuronally associated GO terms (Fig. 4d and Supplementary Tables 5 and 10). These results suggest that the expression of many neuronal genes might require binding of both EGL-43 and FOS-1.

To test this idea, we generated animals expressing endogenous FOS-1::TagRFP-T::AID* and visualized synaptic markers upon FOS-1 degradation. Degradation of FOS-1 caused a 99% reduction in ELKS-1 intensity, with synapses becoming detectable only with increased thresholding (Fig. 4e,f). Similarly, but to a lesser extent, we observed a 55% reduction in RAB-3 intensity (Fig. 4g,h). To test if the direct binding of FOS-1 to synaptic genes is critical for their expression, we deleted the AP-1/FOS-1 site upstream of *elks-1*. Loss of this site dramatically reduced ELKS-1 intensity, phenocopying loss of FOS-1 (Fig. 4e,f). Together, these data demonstrate that both FOS-1 and EGL-43 directly regulate presynaptic gene expression in PDE.

Because FOS-1 is expressed ubiquitously and EGL-43 is expressed in many neurons, including multiple head neurons (Fig. 2c and Supplementary Fig. 2b), we tested the requirement of EGL-43 and FOS-1 on presynaptic gene expression in the nerve ring, the *C. elegans* neuropil. The nerve ring is situated in the head of the animal and contains the majority of the worm's synapses, as labeled by SYD-2/Liprin-α, a major structural component of active zones[10] (Supplementary Fig. 9a). Auxin-induced degradation of either EGL-43 or FOS-1 for 48 h resulted in a 17% and 21% reduction of endogenous SYD-2, respectively (Supplementary Fig. 9b). Next, we tested the requirement of EGL-43 on *rpm-1*/Highwire/Pam, a RING E3 ubiquitin ligase that functions in parallel with SYD-2 to regulate synapse formation[33]. We did not detect any changes in endogenous RPM-1 expression upon EGL-43 degradation (Supplementary Fig. 9c). Thus, EGL-43 and FOS-1 control the expression of specific subsets of synaptic genes, as opposed to broadly affecting pan-neuronal gene expression.

EGL-43 participates in a positive feedback loop with FOS-1

Because both EGL-43 and FOS-1 bind and activate synaptic genes, we investigated the interplay between them. We degraded FOS-1 beginning in L2 and imaged EGL-43::GFP in L4. Loss of FOS-1 led to a slight but significant decrease of EGL-43 in PDE (Fig. 5a,b). This result, together with the data in Fig. 4a,b, suggests that *egl-43* and *fos-1* participate in a positive feedback loop where their expression is partially dependent on each other.

In *C. elegans*, the FOS-1/AP-1 conserved binding motif is a perfect palindrome of 5′-TGACTCA-3′ and is highly homologous to the binding motif of mammalian FOS (Fig. 5c). The FOS-1/AP-1 site upstream of *egl-43* deviates from the consensus by a single nucleotide (5′-TTACTCA-3′), which is conserved across other *Caenorhabditis* species (Supplementary Fig. 10)[22]. Previous computational work on TF binding site mutations predicts that mutation of the FOS site at this position results in a 30% decrease in binding affinity (Fig. 5d)[34]. We wondered if changing this suboptimal FOS-1 site to the consensus sequence would affect the expression of *egl-43*. Using genome editing, we mutated a single nucleotide within the FOS-1 site from 5′-TTACTCA-3′ to 5′-TGACTCA-3′ in animals carrying endogenous EGL-43::GFP. This manipulation dramatically increased EGL-43 intensity in both PVD and PDE (denoted

as gain-of-function (*gof*); Fig. 5e,f), suggesting that *egl-43* activation is highly dependent on FOS-1 binding. Consequently, PDE axons of *egl-43(gof)* animals exhibited increased intensity of ELKS-1 and RAB-3 by 76% and 40%, respectively (Fig. 5g–j). These results illustrate the intricate molecular regulation between *egl-43* and *fos-1* and demonstrate that EGL-43 levels are critical for maintaining optimal levels of presynaptic gene expression.

Manipulation of EGL-43/FOS-1 impacts a behavioral circuit

Because we observed large changes in synaptic protein intensity through our manipulations, we investigated whether there was a functional consequence to these changes in behavior. All *C. elegans* dopaminergic neurons are mechanosensitive and sense stimuli from their food, bacteria[35]. Upon contacting bacteria, the neurons activate and trigger the basal slowing response, an adaptive mechanism that attenuates locomotion to increase time spent in the presence of food[35]. Previous studies revealed that artificial activation of dopaminergic neurons using ChR2 induces backing behavior[36,37].

In the presence of food, we expressed a dopaminergic-specific ChR2 transgene to activate dopaminergic neurons. Constant blue light stimulation elicited a backing response followed by a reversal in wild-type worms, consistent with the literature (Fig. 6a)[37]. We assayed each worm five times, with 15 s between each trial, and measured the time from the onset of light to backward locomotion. Wild-type animals performed backing in 1.85 ± 0.22 s (Fig. 6a). Animals reared in the absence of all-trans-retinal (ATR), the ChR2 cofactor, did not elicit any backing in response to light within 8 s ($n > 50$). Next, we assayed *egl-43(gof)* animals that possess increased levels of EGL-43. Animals responded to light in 1.40 ± 0.43 s, significantly faster than the wild type (Fig. 6b). Thus, increasing EGL-43 expression and increasing synaptic protein levels accelerate the activation of a behavioral circuit.

Because the loss of EGL-43 or FOS-1 strongly reduces presynaptic gene expression, we wondered if their losses would similarly affect the ChR2-induced backing response. We degraded EGL-43 or FOS-1 at L2 and assayed animals at L4. Loss of EGL-43 or FOS-1 dramatically delayed response time, where time to backing was 3.3 ± 1.27 s and 4.3 ± 1.17 s, respectively (Fig. 6c). Collectively, our experiments demonstrate that EGL-43 and FOS-1 directly control presynaptic gene expression, ultimately influencing the strength of synaptic signaling in dopaminergic circuits.

EGL-43 activates activity-regulated and developmental TFs

Having demonstrated that EGL-43 can promote the expression of FOS-1 to modulate presynaptic gene expression, we explored if EGL-43 activates other activity-regulated TFs. We observed EGL-43 ChIP–seq peaks at the *jun-1/Jun*, *crh-1/Creb*, *egrh-1/Egr1* and *mef-2/Mef2* loci and used genome editing to fluorescently tag each TF. All four TFs are expressed broadly, similar to *fos-1* (Fig. 7a–d). We performed auxin-induced degradation of EGL-43 beginning in L2 and examined TFs at L4. Remarkably, loss of EGL-43 increased JUN-1 expression, opposite to our observations with FOS-1, suggesting that EGL-43 might negatively regulate *jun-1* (Fig. 7a). Different from *jun-1*, loss of EGL-43 decreased CRH-1 and EGRH-1 (Fig. 7b,c) but did not significantly affect MEF-2 expression (Fig. 7d). Because MEF2 is implicated in activity-dependent synapse
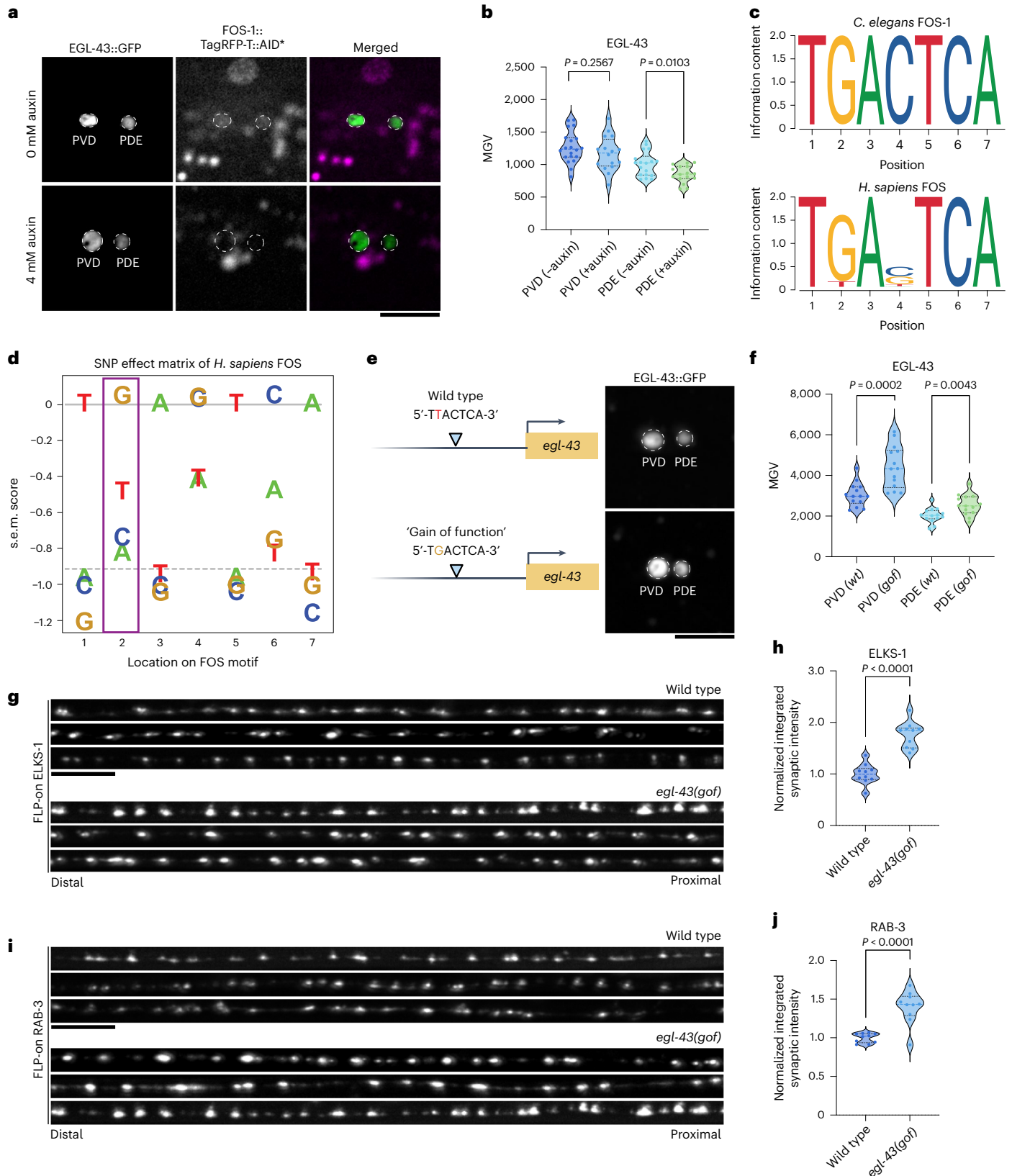

Fig. 5 | FOS-1 modulates *egl-43* expression. a, L4 animals carrying EGL-43::GFP and FOS-1::TagRFP-T::AID* were treated with 0 mM or 4 mM auxin for 48 h to degrade FOS-1. PVD and PDE nuclei are outlined (white dashed circles). **b**, Quantification of EGL-43::GFP intensity shown in **a** ($n = 16$ for both conditions). **c**, JASPAR TF binding profiles for *C. elegans* FOS-1 (top) and *H. sapiens* FOS (bottom). **d**, SNP effect matrix of *H. sapiens* FOS. The purple rectangle highlights the position of the consensus FOS motif that differs in wild-type *C. elegans*. **e**, EGL-43::GFP expression in either the wild type or in animals carrying a gain-of-function (denoted as *egl-43(gof)*) mutation in their FOS-1-binding site upstream of the *egl-43*. PVD and PDE nuclei are outlined (white dashed circles). This schematic was created with BioRender.com. **f**, Quantification of EGL-43::GFP intensity shown in **e** ($n = 14$ for both conditions). **g**, Line scans of FLP-on ELKS-1 in the PDE axon in the wild type and animals carrying *egl-43(gof)*. **h**, Quantification of line scans of animals shown in **g** ($n = 10$ for both conditions, $P = 5.45276 \times 10^{-7}$). **i**, Line scans of FLP-on RAB-3 in the PDE axon in the wild type and animals carrying *egl-43(gof)*. **j**, Quantification of line scans of animals shown in **i** ($n = 10$ for both conditions, $P = 2.18919 \times 10^{-5}$). For all graphs, medians are represented in thick dashed lines and quartiles are represented in thin dashed lines. P values displayed in this figure were calculated using two-tailed unpaired Student's *t* tests. Scale bar for all images $= 10$ μm.

elimination[38], we wondered if MEF-2 functions in opposition to EGL-43 to control synaptogenesis. Using genome editing, we generated a full deletion of *mef-2* but found no significant differences in synaptic markers in PDE (Supplementary Fig. 11a–d). Our findings suggest that EGL-43 controls a specific network of activity-regulated TFs, where CRH-1 and

EGRH-1 might function together with FOS-1 to control presynaptic gene expression.

Genetic screens in *C. elegans* have identified multiple terminal selectors that are critical for dopaminergic identity. Mutations in three genes, *ceh-43*/*Dlx*, *ast-1*/Etv1 and *ceh-20*/*Pbx*, all result in the

a EGL-43::GFP / FOS-1::TagRFP-T::AID* / Merged (0 mM auxin, 4 mM auxin) PVD, PDE

b EGL-43 — MGV; $P = 0.2567$ (PVD −auxin vs PVD +auxin), $P = 0.0103$ (PDE −auxin vs PDE +auxin)

c *C. elegans* FOS-1 and *H. sapiens* FOS — Information content vs Position

d SNP effect matrix of *H. sapiens* FOS — s.e.m. score vs Location on FOS motif

e Wild type 5′-TT**A**CTCA-3′ / 'Gain of function' 5′-T**G**ACTCA-3′ → *egl-43*; EGL-43::GFP, PVD PDE

f EGL-43 — MGV; $P = 0.0002$ (PVD (wt) vs PVD (gof)), $P = 0.0043$ (PDE (wt) vs PDE (gof))

g FLP-on ELKS-1 — Wild type / *egl-43(gof)*; Distal, Proximal

h ELKS-1 — Normalized integrated synaptic intensity; $P < 0.0001$ (Wild type vs *egl-43(gof)*)

i FLP-on RAB-3 — Wild type / *egl-43(gof)*; Distal, Proximal

j RAB-3 — Normalized integrated synaptic intensity; $P < 0.0001$ (Wild type vs *egl-43(gof)*)

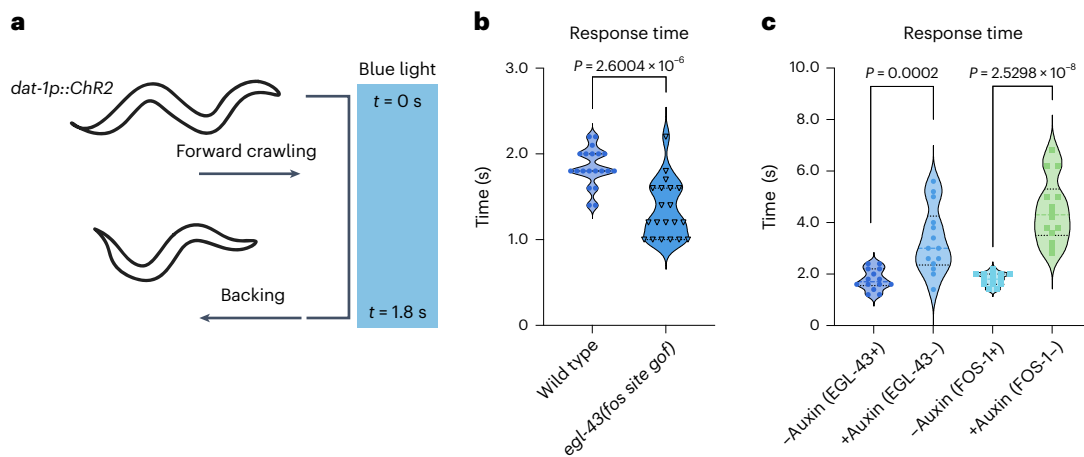**Fig. 6 | A dopaminergic behavioral circuit is dependent on EGL-43 and FOS-1 expression. a**, Schematic representation of the backing assay. ChR2 was specifically expressed in dopaminergic neurons using the *dat-1* promoter. Healthy, fed worms move forward, foraging on a bacterial lawn. On constant excitation by blue light, dopaminergic neurons activate and induce a backing response, followed by a reversal. The time from the onset of the blue light to a backing response was recorded. Wild-type worms perform the backing behavior in under 2 s under our conditions. **b**, Animals carrying a mutation to enhance FOS-1 binding upstream of the *egl-43* locus exhibit a faster backing response than the wild type ($n = 20$ for both conditions, $P = 2.60044 \times 10^{-6}$). **c**, Auxin-induced degradation of either EGL-43 or FOS-1 results in a significantly slower backing response. $n = 14$ for all conditions tested; $P = 0.0002$ (−auxin versus +auxin for EGL-43), $P = 2.52982 \times 10^{-8}$ (−auxin versus +auxin for FOS-1). For all graphs, medians are represented in thick dashed lines, and quartiles are represented in thin dashed lines. P values were calculated using two-tailed unpaired Student's t tests.

loss of dopaminergic identity markers such as DAT-1 but do not affect the expression of pan-neuronal markers such as RAB-3 (refs. 39,40). Additionally, *unc-62/Meis* functions together with terminal selectors in PDE to specify dopaminergic identity[41]. Because degradation of EGL-43 results in the loss of both DAT-1 and RAB-3 expression, we asked if EGL-43 acts upstream of these TFs. We observed EGL-43 ChIP–seq peaks present at all four genes and used genome editing to fluorescently tag each TF. Degradation of EGL-43 reduced the expression of all four TFs in PDE, indicating that EGL-43 modulates terminal selector expression (Fig. 7e–h). Others have reported that the loss of individual terminal selectors results in only partial loss of DAT-1 due to compensation by other terminal selectors[39,40]. However, we found that degradation of EGL-43 resulted in a complete loss of DAT-1 in PDE, consistent with our data that EGL-43 functions upstream.

Unlike terminal selectors, CUT TFs are expressed throughout the nervous system and bind and regulate pan-neuronal genes, such as *rab-3* (ref. 3). We observed EGL-43 ChIP–seq peaks near all CUT genes, and we tested the requirement of EGL-43 on four previously described tagged CUT alleles[3]. Degradation of EGL-43 significantly reduced CEH-41 and CEH-48 expression, but not CEH-38 and CEH-44 (Fig. 7i–l), indicating that EGL-43 controls specific CUTs in PDE. We then investigated the synergy between EGL-43 and CUTs to control RAB-3 expression. Using genome editing, we mutated the CUT, EGL-43 or both motifs upstream of *rab-3* and imaged PDE axons at L4. These mutations resulted in similar decreases in RAB-3 intensity, suggesting that EGL-43 and CUTs might function in the same pathway to activate pan-neuronal genes.

Discussion

During development, synapses assemble in a rapid and organized fashion. To accomplish this, neurons use spontaneous and sensory-driven activity-dependent mechanisms to drive the transcription of specific genes. Using a model neuron, we discovered that EGL-43/MECOM and FOS-1/FOS function together to drive synapse formation. First, we found that both TFs bind promoters of many synaptic genes. Second, depletion of either TF reduces synaptic protein levels. Third, mutation of either TF's binding sites in synaptic genes reduces synaptic protein levels. Finally, EGL-43 modulates the expression of genetic programs that constitute different aspects of neuronal identity.

Notably, bidirectionally manipulating activity impacts FOS-1 expression and subsequent synaptic protein expression, suggesting that activity-dependent mechanisms for synaptogenesis use the EGL-43/FOS-1 program.

In addition to directly activating presynaptic genes, EGL-43 and FOS-1 function in a positive feedback loop. They each bind to the promoter of the other gene and are mutually required for their expression. Optimizing the FOS-1 site upstream of *egl-43* profoundly increased EGL-43 levels, resulting in increased synaptic signaling and behavioral changes. Remarkably, the suboptimal site is conserved across millions of years of evolution[22], suggesting positive selection pressure to maintain particular levels of EGL-43, and thus FOS-1, for survival.

Presynaptic assembly is a complex biological process that involves transcription of active zone and synaptic vesicle genes, selective expression of neurotransmitter phenotype-related genes and specification of presynaptic membrane by transsynaptic adhesion molecules. Recent work in *C. elegans* revealed that CUT TFs regulate pan-neuronal gene expression and function together with terminal selectors to define neuronal identity and function[3]. One important question is how these hardwired genetic programs are regulated to ensure functional connectivity between neurons.

We propose that during development, pro-neuronal signaling activates EGL-43 to generate a robust activity-regulated gene expression program (Fig. 8). Here EGL-43 activates both terminal selectors and CUTs to execute expression of key neuronal genes. Simultaneously, EGL-43 and FOS-1 bind to presynaptic genes to modulate their expression. Notably, EGL-43 participates in a positive feedback loop with FOS-1, which is activated by neuronal activity. We hypothesize that during synaptogenesis, activity stimulates the EGL-43/FOS-1 loop, modulating presynaptic gene expression.

Strikingly, we found that EGL-43 is expressed predominantly in sensory neurons. Sensory neurons constantly monitor the environment, where their signaling leads to behavioral changes. For example, the thermosensory amphid finger (AFD) neuron uses short-term transcription-independent and long-term transcription and experience-dependent plasticity mechanisms to modulate behavior in response to environmental temperature[42]. Because the EGL-43/FOS-1 program can rapidly activate synaptic genes, it is plausible that sensory neurons use this program to enable plasticity and fine-tune
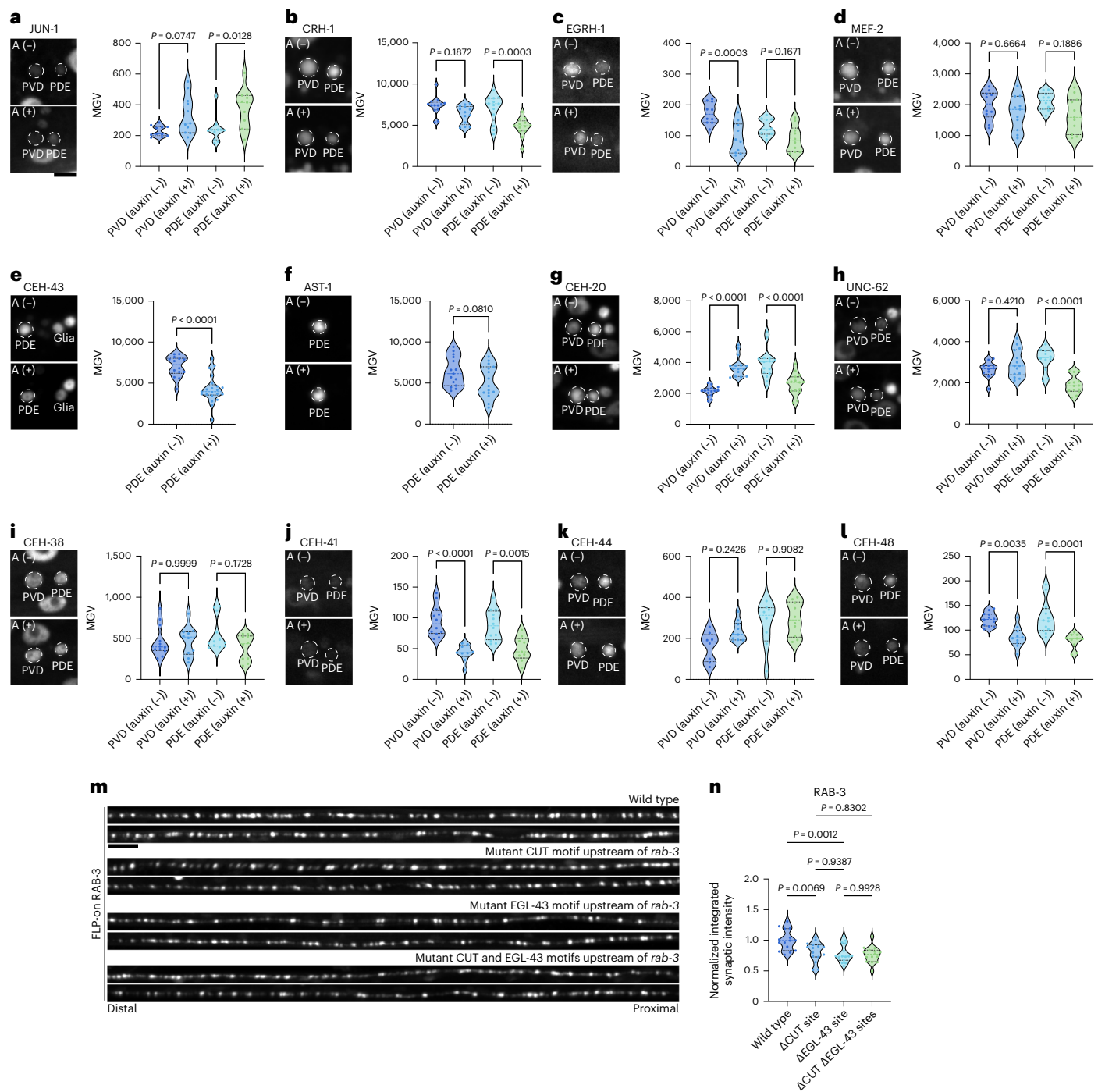
Fig. 7 | EGL-43 regulates the expression of activity-dependent TFs and hardwired genetic pathways to promote presynaptic gene expression.
a–l, Left: images of L4 animals carrying endogenously tagged GFP or mNG TFs and EGL-43::TagRFP-T::AID* treated with 0 mM (A(−)) or 4 mM auxin (A(+)) for 48 h. PVD and PDE neuronal nuclei are outlined (white dashed circles). Right: quantification of TF intensity in the images shown on the left. Classification of the following factors tested with sample sizes: activity-dependent TFs JUN-1, $n = 11$ (A−) and $n = 11$ (A+) (**a**); CRH-1, $n = 13$ (A−) and $n = 13$ (A+) (**b**); EGRH-1, $n = 10$ (A−) and $n = 10$ (A+) (**c**); MEF-2, $n = 10$ (A−) and $n = 11$ (A+) (**d**). Classification of the following dopaminergic terminal selectors/associated factors: CEH-43, $n = 14$ (A−), $n = 21$ (A+), $P = 8.6174 \times 10^{-6}$ (**e**); AST-1, $n = 15$ (A−), $n = 15$ (A+) (**f**); CEH-20, $n = 15$ (A−), $n = 15$ (A+), $P = 3.84033 \times 10^{-11}$ (PDE) (**g**); UNC-62, $n = 12$ (A−), $n = 14$

(A+), $P = 1.15877 \times 10^{-12}$ (PVD), $P = 2.78114 \times 10^{-8}$ (PDE) (**h**). CUT homeobox TFs are as follows: CEH-38, $n = 12$ (A−), $n = 10$ (A+) (**i**); CEH-41, $n = 12$ (A−), $n = 9$ (A+), $P = 4.09353 \times 10^{-9}$ (PVD) (**j**); CEH-44 $n = 8$ (A−), $n = 10$ (A+) (**k**); CEH-48, $n = 12$ (A−), $n = 10$ (A+) (**l**). **m**, Line scans of PDE axons from animals expressing endogenous FLP-on RAB-3. Mutations were generated in the promoter of *rab-3* corresponding to the CUT, EGL-43 or both CUT and EGL-43 motifs. **n**, Quantification of the line scans shown in **m** ($n = 15$ for all genotypes). For all graphs, medians are represented in thick dashed lines, and quartiles are represented in thin dashed lines. P values were calculated using ordinary one-way ANOVA except for **e** and **f**, which were calculated using two-tailed unpaired Student's t tests. Scale bar = 5 μm for images of nuclei; scale bar = 10 μm for line scans of PDE axons.
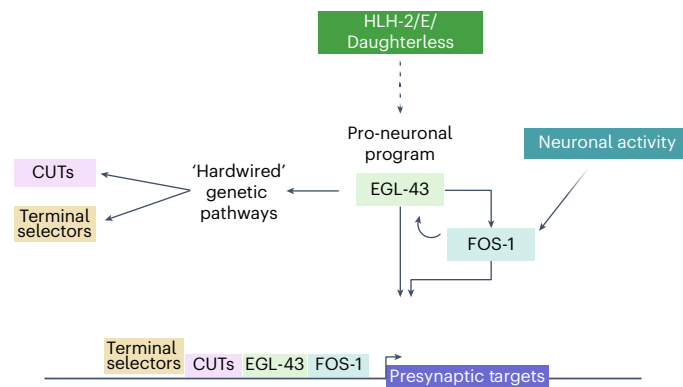
Fig. 8 | A model for the role of EGL-43 in dopaminergic neurons. EGL-43 functions downstream of the initial pro-neuronal fate commitment and is a key organizer of synaptogenesis in dopaminergic neurons. Together with the activity-dependent TF FOS-1, EGL-43 functions in a positive feedback loop and binds upstream regulatory regions of synaptic targets to promote gene expression. Simultaneously, EGL-43 promotes the expression of hardwired genetic programs, such as terminal selector and pan-neuronal (CUT) TFs, that in turn also bind presynaptic loci and promote transcription through the same pathway. We hypothesize that during development, neuronal activity can modulate the strength of synaptic gene expression through EGL-43 and FOS-1 to ensure functional connectivity. This schematic was created with BioRender.com.

behavior. Unlike sensory neurons, we did not detect EGL-43 in any motoneurons. The *C. elegans* motoneurons are a critical component of the locomotion circuit, which generates stereotyped forward and backward movement. Compared to the myriads of sensory modality, the wide range of stimulus intensity and rapid changes in response, the locomotion program is relatively simple and rigid, and thus may not require the plasticity mechanisms enabled by EGL-43.

A large body of evidence supports the notion that activity shapes synaptic connectivity during development[4]. Activity-regulated TFs, such as CREB, FOS and JUN, have important roles in this process. Here we demonstrate that FOS-1 directly activates presynaptic genes, providing a potential mechanism that underlies activity-regulated modification of synaptic circuits. In vertebrates, the majority of AP-1/FOS sites reside in enhancer regions[43]. Conversely, due to its compact genome size, *C. elegans* FOS-1 sites are found near TSSs[44]. While future experiments are needed to determine whether FOS can directly control synaptic programs in vertebrates, our work identifies a crucial link between activity and genetic programs to modulate synaptic gene expression.

Online content

Any methods, additional references, Nature Portfolio reporting summaries, source data, extended data, supplementary information, acknowledgements, peer review information; details of author contributions and competing interests; and statements of data and code availability are available at https://doi.org/10.1038/s41593-024-01728-x.

References

1. Deguchi, Y., Donato, F., Galimberti, I., Cabuy, E. & Caroni, P. Temporally matched subpopulations of selectively interconnected principal neurons in the hippocampus. *Nat. Neurosci.* **14**, 495–504 (2011).
2. Hobert, O. & Kratsios, P. Neuronal identity control by terminal selectors in worms, flies, and chordates. *Curr. Opin. Neurobiol.* **56**, 97–105 (2019).
3. Leyva-Diaz, E. & Hobert, O. Robust regulatory architecture of pan-neuronal gene expression. *Curr. Biol.* **32**, 1715–1727 (2022).
4. Andreae, L. C. & Burrone, J. The role of neuronal activity and transmitter release on synapse formation. *Curr. Opin. Neurobiol.* **27**, 47–52 (2014).
5. Wiesel, T. N. & Hubel, D. H. Single-cell responses in striate cortex of kittens deprived of vision in one eye. *J. Neurophysiol.* **26**, 1003–1017 (1963).
6. Greenberg, M. E., Ziff, E. B. & Greene, L. A. Stimulation of neuronal acetylcholine receptors induces rapid gene transcription. *Science* **234**, 80–83 (1986).
7. Lanahan, A. & Worley, P. Immediate-early genes and synaptic function. *Neurobiol. Learn. Mem.* **70**, 37–43 (1998).
8. Herdegen, T. & Leah, J. D. Inducible and constitutive transcription factors in the mammalian nervous system: control of gene expression by Jun, Fos and Krox, and CREB/ATF proteins. *Brain Res. Rev.* **28**, 370–490 (1998).
9. Sheng, M. & Greenberg, M. E. The regulation and function of c-fos and other immediate early genes in the nervous system. *Neuron* **4**, 477–485 (1990).
10. McDonald, N. A., Fetter, R. D. & Shen, K. Assembly of synaptic active zones requires phase separation of scaffold molecules. *Nature* **588**, 454–458 (2020).
11. Schwartz, M. L. & Jorgensen, E. M. SapTrap, a toolkit for high-throughput CRISPR/Cas9 gene modification in *Caenorhabditis elegans*. *Genetics* **202**, 1277–1288 (2016).
12. Pokala, N., Liu, Q., Gordus, A. & Bargmann, C. I. Inducible and titratable silencing of *Caenorhabditis elegans* neurons in vivo with histamine-gated chloride channels. *Proc. Natl Acad. Sci. USA* **111**, 2770–2775 (2014).
13. Maeder, C. I. et al. The THO complex coordinates transcripts for synapse development and dopamine neuron survival. *Cell* **174**, 1436–1449 (2018).
14. Nagel, G. et al. Light activation of channelrhodopsin-2 in excitable cells of *Caenorhabditis elegans* triggers rapid behavioral responses. *Curr. Biol.* **15**, 2279–2284 (2005).
15. Birdwell, C. et al. EVI1 dysregulation: impact on biology and therapy of myeloid malignancies. *Blood Cancer J.* **11**, 64 (2021).
16. Chen, P. et al. MECOM promotes supporting cell proliferation and differentiation in cochlea. *J. Otol.* **17**, 59–66 (2022).
17. Wang, Z. et al. EVI1 overexpression promotes ovarian cancer progression by regulating estrogen signaling. *Mol. Cell Endocrinol.* **534**, 111367 (2021).
18. Leszczynski, P. et al. Deletion of the *Prdm3* gene causes a neuronal differentiation deficiency in P19 cells. *Int. J. Mol. Sci.* **21**, 7192 (2020).
19. Kazama, H., Kodera, T., Shimizu, S., Mizoguchi, H. & Morishita, K. Ecotropic viral integration site-1 is activated during, and is sufficient for, neuroectodermal P19 cell differentiation. *Cell Growth Differ.* **10**, 565–573 (1999).
20. Garriga, G., Guenther, C. & Horvitz, H. R. Migrations of the *Caenorhabditis elegans* HSNs are regulated by *egl-43*, a gene encoding two zinc finger proteins. *Genes Dev.* **7**, 2097–2109 (1993).
21. Hwang, B. J., Meruelo, A. D. & Sternberg, P. W. *C. elegans* EVI1 proto-oncogene, EGL-43, is necessary for Notch-mediated cell fate specification and regulates cell invasion. *Development* **134**, 669–679 (2007).
22. Rimann, I. & Hajnal, A. Regulation of anchor cell invasion and uterine cell fates by the egl-43 Evi-1 proto-oncogene in *Caenorhabditis elegans*. *Dev. Biol.* **308**, 187–195 (2007).
23. Medwig-Kinney, T. N. et al. A developmental gene regulatory network for *C. elegans* anchor cell invasion. *Development* **147**, dev185850 (2020).
24. Deng, T. et al. The *Caenorhabditis elegans* homolog of the Evi1 proto-oncogene, egl-43, coordinates G1 cell cycle arrest with pro-invasive gene expression during anchor cell invasion. *PLoS Genet.* **16**, e1008470 (2020).
25. Grove, C. A. et al. A multiparameter network reveals extensive divergence between *C. elegans* bHLH transcription factors. *Cell* **138**, 314–327 (2009).

26. Ashley, G. E. et al. An expanded auxin-inducible degron toolkit for *Caenorhabditis elegans*. *Genetics* **217**, iyab006 (2021).

27. Tang, J. L. Y. et al. NanoDam identifies homeobrain (ARX) and scarecrow (NKX2.1) as conserved temporal factors in the *Drosophila* central brain and visual system. *Dev. Cell* **57**, 1193–1207 e1197 (2022).

28. Yee, C. et al. A NanoDam toolkit for tissue-specific transcription factor profiling in *C. elegans*. Preprint at *bioRxiv* https://doi.org/10.1101/2023.05.31.543105 (2023).

29. Delwel, R., Funabiki, T., Kreider, B. L., Morishita, K. & Ihle, J. N. Four of the seven zinc fingers of the Evi-1 myeloid-transforming gene are required for sequence-specific binding to GA(C/T)AAGA(T/C)AAGATAA. *Mol. Cell Biol.* **13**, 4291–4300 (1993).

30. Yoshimi, A. et al. Evi1 represses PTEN expression and activates PI3K/AKT/mTOR via interactions with polycomb proteins. *Blood* **117**, 3617–3628 (2011).

31. West, A. E. & Greenberg, M. E. Neuronal activity-regulated gene transcription in synapse development and cognitive function. *Cold Spring Harb. Perspect. Biol.* **3**, a005744 (2011).

32. Chung, S. H. et al. Novel DLK-independent neuronal regeneration in *Caenorhabditis elegans* shares links with activity-dependent ectopic outgrowth. *Proc. Natl Acad. Sci. USA* **113**, E2852–E2860 (2016).

33. Opperman, K. J. & Grill, B. RPM-1 is localized to distinct subcellular compartments and regulates axon length in GABAergic motor neurons. *Neural Dev.* **9**, 10 (2014).

34. Nishizaki, S. S. et al. Predicting the effects of SNPs on transcription factor binding affinity. *Bioinformatics* **36**, 364–372 (2020).

35. Sawin, E. R., Ranganathan, R. & Horvitz, H. R. *C. elegans* locomotory rate is modulated by the environment through a dopaminergic pathway and by experience through a serotonergic pathway. *Neuron* **26**, 619–631 (2000).

36. Kindt, K. S. et al. Dopamine mediates context-dependent modulation of sensory plasticity in *C. elegans*. *Neuron* **55**, 662–676 (2007).

37. Vidal-Gadea, A. et al. *Caenorhabditis elegans* selects distinct crawling and swimming gaits via dopamine and serotonin. *Proc. Natl Acad. Sci. USA* **108**, 17504–17509 (2011).

38. Flavell, S. W. et al. Activity-dependent regulation of MEF2 transcription factors suppresses excitatory synapse number. *Science* **311**, 1008–1012 (2006).

39. Doitsidou, M. et al. A combinatorial regulatory signature controls terminal differentiation of the dopaminergic nervous system in *C. elegans*. *Genes Dev.* **27**, 1391–1405 (2013).

40. Flames, N. & Hobert, O. Gene regulatory logic of dopamine neuron differentiation. *Nature* **458**, 885–889 (2009).

41. Jimeno-Martin, A. et al. Joint actions of diverse transcription factor families establish neuron-type identities and promote enhancer selectivity. *Genome Res.* **32**, 459–473 (2022).

42. Goodman, M. B. & Sengupta, P. The extraordinary AFD thermosensor of *C. elegans*. *Pflugers Arch.* **470**, 839–849 (2018).

43. Vierbuchen, T. et al. AP-1 transcription factors and the BAF complex mediate signal-dependent enhancer selection. *Mol. Cell* **68**, 1067–1082 (2017).

44. Kudron, M. M. et al. The ModERN resource: genome-wide binding profiles for hundreds of *Drosophila* and *Caenorhabditis elegans* transcription factors. *Genetics* **208**, 937–949 (2018).

Methods

C. elegans culture and maintenance

Nematodes were cultured under normal conditions on nematode growth media (NGM) plates seeded with *Escherichia coli* OP50 at 20 °C. To make histamine plates, histamine dihydrochloride (Sigma-Aldrich) was dissolved in water to generate a 1 M stock solution. Fresh histamine stock solution was added to molten NGM agar at approximately 65 °C to a final concentration of 10 mM. The worm strains used in this study are listed in Supplementary Table 13. All experiments used hermaphrodite worms, and the stages used for each experiment are outlined in each figure legend.

Auxin depletion

NGM plates were supplemented to a final concentration of 4 mM K-NAA (auxin salt; PhytoTech Labs) from a 1 M stock solution. Auxin-containing plates were seeded using OP50 bacteria and stored at 4 °C for up to 2 weeks before use. Well-fed hermaphrodite worms were moved onto seeded auxin plates at the L2 stage and imaged at the L4 stage, unless otherwise noted.

Molecular biology, cloning and microinjection

For genotyping, worms were lysed in worm lysis buffer as previously described. Worm lysates were amplified using either SuperFi II Master Mix (Thermo Fisher Scientific) or CloneAmp (Takara). To generate pCY37 (*dat-1p::ChR2*), a fragment containing the *dat-1* promoter was digested from pCM558 (*dat-1p::Cre*) using *SphI* and *AscI* and purified using a Qiagen Gel Extraction Kit. pTLs30 (*ser-2prom3::ChR2::unc-54 3′UTR*) was digested with *SphI* and *AscI*, and the vector backbone containing ChR2 was similarly purified. The resulting two fragments were ligated together overnight using T4 ligase (Thermo Fisher Scientific). Transgenes were generated using standard gonad transformation by injection.

Genome editing by CRISPR–Cas9

For fluorophore insertions, primers providing at least 50 nucleotides of homology to the genomic locus were used to amplify PCR repair templates. Plasmids pWZ203 (TagRFP-T::AID*), pCM552 (GFPnovo2), pJW2098 (mScarlet::AID*) and pJW2171 (mNeonGreen::AID*) were used as templates for PCR repair products. CloneAmp PCR reactions with a volume of 4 × 50 µl were performed to generate repair products, which were subsequently pooled and purified together using a Qiagen PCR Purification Kit. PCR products were eluted in 10 µl of water and quantified using a NanoDrop instrument (Thermo Fisher Scientific). PCR templates were melted immediately before use, as previously described. For binding site mutations, long primers (<100 nucleotides (nt); Thermo Fisher Scientific) and ultramers/gBlocks (>100 nt; Integrated DNA Technologies (IDT)) were resuspended in water to a concentration of 100 µM.

cRNAs (IDT) were resuspended to a stock concentration of 100 µM in duplex buffer (IDT). In total, 0.5 µl of 100 µM cRNA was added to a tube containing 3 µl of 10 µM tracrRNA and heated in a PCR machine at 95 °C for 5 min followed by 25 °C for 5 min. The cRNA:tracrRNA reaction was transferred to a 1.5 ml tube containing 0.5 µl of ALT-R Cas9 enzyme and heated in a 37 °C water bath for 15 min. In total, 5 µl of freshly melted PCR product was added to the tube (final concentration = ~300 ng µl⁻¹), with 1 µl of co-injection plasmid (pRF4, final concentration = 50 ng µl⁻¹) to bring the volume of the injection mixture to 10 µl. Injection mixes were spun at 13,000 rpm for 15 min and subsequently kept on ice during microinjection. Details of individual CRISPR edits (guides, oligos and locations) are found in Supplementary Table 11. In many cases, it was necessary to mutate the PAM site to prevent Cas9 from editing the repair template, where NGG was mutated to NGT.

Neuronal silencing and activation

For neuronal silencing experiments, wyEx8629 (*dat-1p::HisCl1*) worms were placed on plates containing 0 or 10 mM histamine seeded with OP50. At 20 °C, hermaphrodite worms were placed on histamine plates at the L2 stage and observed at the L4 stage.

For neuronal activation experiments, all worms were crossed into a *lite-1(ce314)* background and were grown at 20 °C on plates with OP50 mixed with or without ATR. ATR (Sigma-Aldrich) was dissolved in pure ethanol to create a 100 mM stock concentration, which was stored at −20 °C. In total, 5 µl of the 100 mM ATR stock was added to 1 ml of OP50 culture, and 100 µl was added to NGM plates. Plates were kept in the dark and used the following day. Worms carrying *wyEx10629* and *wyEx10630* were grown in the presence of ATR and stimulated using blue light emitted from a SOLA Light Engine (Lumencor) pulsed for ten cycles of 15 s (on) and 60 s (off). For FOS-1::GFP imaging experiments, worms were treated with blue light at L2 and allowed to recover for 2 h before imaging. For imaging FLP-on::GFP::ELKS-1, worms were treated with blue light at L2 and imaged at L4. For the neuronal activation backing/reversal assays, free, forward-moving worms were stimulated using constant blue light using a SOLA Light Engine. A timer was used to measure the time required from the onset of blue light until a backing response was invoked. Each animal was assayed five times, with 15 s rest between trials.

Microscopy and imaging

Worms were mounted on 3% agarose pads made by melting agarose in M9 buffer. Worms were immobilized using 10 mM levamisole, which was diluted in M9 buffer. Imaging was performed either on a Zeiss Axio Observer Z1 microscope paired with a Yokogawa CSU-X1 spinning-disk unit and a Hamamatsu EM-CCD digital camera controlled by Metamorph (v.7.8.12.0) and using either a Plan-Apochromat ×100 (1.4 numerical aperture (NA)) objective or a ×63 (1.4 NA) objective or on an inverted Zeiss Axio Observer Z1 microscope paired with a Yokogawa CSU-W1 spinning-disk unit and a Prime 95B Scientific CMOS camera with a C-Apochromat ×40 (0.9 NA) objective with ×1 or ×2 enhanced digital magnification controlled by 3i Slidebook (v6) software. Image settings (laser power and exposure time) were identical for all genotypes or treatments across experiments. Images were taken typically with 1 um step sizes in *z* stacks of 20–30 µm range.

Raw image files were processed using Fiji (ImageJ) software. For synapse analyses, image stacks were *z* projected using maximum projection, and axons were straightened using the plugin 'straighten to line' to generate line scans. Images were thresholded and analyzed identically using the 'analyze particles' function, where axon length and integrated synapse intensity were measured as previously described[13]. The integrated intensity for each synapse (particle) was then summed and finally divided by PDE axon length to obtain an intensity per µm value. For normalization, all intensity per µm values corresponding to the control group were first averaged to generate a mean intensity per µm value. Each individual value for both control groups and mutant/treated groups was then divided by the control mean intensity per µm value and plotted. For all other measurements, including nerve ring, and nuclei intensities, images were *z*-projected using 'sum' stack. Regions of interest were manually drawn and quantified using the 'measure' function.

RNA extraction and qPCR

Worms were washed thrice in 1.5-ml tubes with M9 buffer and aspirated to remove as much buffer as possible. Worm pellets were flash frozen in liquid nitrogen and thawed thrice to facilitate cracking of the cuticle. Total RNA was extracted using Trizol (Thermo Fisher Scientific) according to manufacturer protocols. cDNA libraries were generated using SuperScript III or SuperScript VILO (Thermo Fisher Scientific), and qPCR was performed on a CFX90 thermocycler (Bio-Rad) using SsoFast EvaGreen Master Mix (Bio-Rad). qPCR results were analyzed using the $2^{-\Delta\Delta CT}$ method.

ChIP–qPCR

Worms were bleach-synchronized and grown at 25 °C until the L3 stage (24 h after placing L1s on food), washed thrice in PBS supplemented

with Complete Mini protease inhibitor (Roche) and flash frozen in liquid nitrogen to make worm popcorn. Worm popcorn was stored at −80 °C until three biological replicates were obtained. Worm popcorn was ground in a mortar in liquid nitrogen, and powder was added to ten volumes of PBS containing 1.1% formaldehyde, Complete Mini protease inhibitor (Roche) and phosphatase inhibitor cocktail (Calbiochem) and incubated for 10 min at room temperature with rocking. Formaldehyde was quenched by adding glycine to a final concentration of 125 mM, and the solution was pelleted and washed in cold PBS supplemented with 1 mM phenylmethylsulfonyl fluoride. The resulting pellet was resuspended in FA buffer (50 mM HEPES/KOH (pH 7.5), 1 mM EDTA, 1% Triton X-100, 0.1% sodium deoxycholate and 150 mM NaCl) supplemented with 0.1% sarkosyl and the aforementioned protease and phosphatase inhibitors. The resuspended pellet was sonicated using an EpiShear probe sonicator (Active Motif) for 2× 13-min intervals at 80% power (30 s on and 30 s off). Following sonication, immunoprecipitation (IP) was performed using GFP-Trap Agarose (ChromoTek) according to manufacturer protocols, with unconjugated agarose beads used as a control. In total, 25 µl was reserved as input DNA. IP and input DNA were purified using ChIP elution buffer (250 mM NaCl, 1% SDS, 10 mM Tris–Cl (pH 8) and 1 mM EDTA) and incubated with proteinase K (Thermo Fisher Scientific) overnight at 65 °C. DNA was purified using a PCR Purification Kit (Qiagen). DNA was quantified using a Qubit dsDNA High Sensitivity Kit and a Qubit 4.0 fluorometer (Thermo Fisher Scientific). qPCR using primers targeting *elks-1* was performed on the resulting purified input and IP DNA using SsoFast EvaGreen SuperMix (Bio-Rad) on a Bio-Rad CFX96 thermocycler. Primers used for these experiments are listed in Supplementary Table 12.

NanoDam profiling
Nematodes carrying a NanoDam driver or both a NanoDam driver and an endogenous GFP-tagged TF were bleached and grown on NGM plates seeded with *E. coli dam*$^{-/-}$ *dcm*$^{-/-}$ lawns. Worms were cultured for at least three generations and then bleach-synchronized and grown at 25 °C for 24 h to obtain synchronized L3 animals. Worms were washed thoroughly in M9 buffer and flash frozen in liquid nitrogen. Worm pellets were stored at −80 °C until needed.

Three biological replicates were obtained for each condition (NanoDam control and NanoDam + GFP allele), and all pellets were processed together to avoid batch effects. gDNA was extracted using a Qiagen DNeasy spin column kit (Qiagen) and resuspended in water. gDNA was digested using DpnI (New England Biolabs), and double-strand adaptors were ligated using T4 DNA Ligase (Thermo Fisher Scientific). Ligated DNA was next amplified using HiDi DNA Polymerase (myPols Biotec) and run on a 1% gel to check for amplification. PCR was performed with four initial long cycles, followed by 20 regular PCR cycles. Amplicons were purified using AMPure magnetic beads (Beckman Coulter) and quantified using a Qubit 4.0 with a Qubit dsDNA High Sensitivity Kit (Thermo Fisher Scientific). Nanopore sequencing libraries were prepared according to manufacturer protocols using a Ligation Sequencing Kit (SQK-LSK-109 (ONT)) and Native Barcoding Expansion Kit (EXP-NBD104 and EXP-NBD114). Nanopore sequencing of pooled libraries was performed on a Nanopore MinION Mk1C device using Spot-ON Flow Cells (v.R9; FLO-MIN106D). Base calling and demultiplexing of fast5 files were performed onboard the MinION MK1C using fast basecalling and a minimum *Q* quality score of 8. Fastq files were mapped to the *C. elegans* ce10 genome using minimap2 and converted to bam using samtools (v.1.14) damidseq_pipeline (v.1.5.3) and find_peaks (v.1.0.1) were used to subsequently call NanoDam peaks.

Flow cytometry and ATAC−seq
Mixed-stage worms carrying a pan-neuronal nuclear GFP (otIs381) transgene were grown at 20 °C and washed thrice with M9 buffer. Nuclei were collected as previously described using a stainless-steel tissue grinder (Wheaton). Suspended nuclei were filtered using 5-µm cell strainers (Corning) and kept on ice. Nuclei were labeled with DAPI (Thermo Fisher Scientific) according to manufacturer instructions and sorted using a BD FACSAria Fusion with a 70 µm nozzle equipped with a blue laser for GFP detection (488 nm, 525/50 filter with B525 detector) and a UV laser for DAPI detection (355 nm, 515/30 filter with U515 detector). The gating strategy is illustrated in Supplementary Fig. 12. Initial FSC and SSC gates were drawn to select against debris, which was verified by imaging on a compound microscope at the Stanford FACS core. Negative GFP gates were generated using N2 animals that did not carry the pan-neuronal marker. Approximately 100,000 positive events were collected for three biological replicates. Samples were spun down and immediately subjected to transposition using Nextera reagents (25 µl tagmentation DNA buffer), 2.5 µl TDE1 and 22.5 µl H$_2$O; Illumina). The transposition reaction was incubated at 37 °C for 30 min, followed by purification using a PCR purification kit (Qiagen). Transposed DNA was next amplified using NEBNext High-Fidelity 2× PCR Master Mix and standard ATAC primers, with an initial qPCR step to determine the cycles required for amplification. PCR products were purified using AMPure magnetic beads (Beckman Coulter) and assayed on an Agilent Bioanalyzer 2100 for quality and success of the ATAC reactions (presence of histone ladder). The resultant Nextera libraries were sequenced on the HiSeq 2000 platform (2 × 101 bp; Illumina) at the Stanford Genome Sequencing Service Center. Fastq reads were trimmed, filtered for quality using FastQC (v.0.11.9), mapped to the *C. elegans* ce10 genome using Bowtie 2 (v.2.5.1) and processed using the standardized ENCODE consortium ATAC−seq pipeline to obtain peaks (atac-seq-pipeline (v.1.14)).

TF peak analysis and Gene Ontology
Because ChIP−seq reads generated many small peaks that are not reflective of the occurrence of GATC fragments used by DamID, we merged processed peaks obtained from the averaged ChIP−seq and NanoDam signals that were within 1,500 bp using bedtools (v.2.28) merge. ChIP−seq and NanoDam peaks for EGL-43 and FOS-1 were processed using HOMER (annotatePeaks, v.4.11) to associate peaks with nearby genes. The resulting gene lists from ChIP−seq and NanoDam experiments were analyzed using the PANTHER overrepresentation test (release: 7 October 2022) with the GO database (release: 1 July 2022) and compared against the *C. elegans* reference list for GO biological process complete terms using Fisher's exact test.

Statistics, data visualization and reproducibility
All data were analyzed either in Microsoft Excel or GraphPad Prism 9. IGV (v.2.15.2) was used to visualize the ATAC−seq and ChIP−seq signals. SeqPlots (v.3.0.12) was used to generate *z*-score aggregation plots for ChIP−seq and NanoDam signals. The protein structure of MECOM-related proteins shown in Fig. 2a was drawn using R Studio (v.4.1.1) and the drawProteins package (v.3.16). For statistical tests, single pairwise comparisons of genotypes or treatments were analyzed using two-tailed unpaired Student's *t* tests. Multiple comparisons were performed using one-way analysis of variance (ANOVA). Data distribution was assumed to be normal, but this was not formally tested. Data collection and analysis were not performed blind to the conditions of the experiments. No data exclusion was performed. No randomization was necessary due to the experimental conditions. No statistical methods were used to predetermine sample sizes, but our sample sizes are similar to those reported in previous publications[3,13]. All imaging data were replicated in at least three independent imaging sessions. All experiments showing representative images were repeated with similar results.

Reporting summary
Further information on research design is available in the Nature Portfolio Reporting Summary linked to this article.

Author contributions

C.Y., D.Q.M. and K.S. conceived and designed the study. Genome editing experiments were performed by C.Y., Y.X. and H.C. Genetics, genomics (ATAC–seq, ChIP and NanoDam), optogenetics and auxin treatment experiments were performed by C.Y. Microscopy was performed by C.Y. and A.R.R. C.Y. and A.P.B. performed computation analyses. B.X. and Y.K.X. provided technical support. T.N.M.-K., W.Z. and W.A.H. contributed to strain and reagent generation. C.Y. wrote the original draft and all authors edited the paper.

Competing interests

The authors declare no competing interests.

Additional information

Supplementary information The online version contains supplementary material available at https://doi.org/10.1038/s41593-024-01728-x.

Correspondence and requests for materials should be addressed to Kang Shen.

Peer review information *Nature Neuroscience* thanks the anonymous reviewers for their contribution to the peer review of this work.

Reprints and permissions information is available at www.nature.com/reprints.

Corresponding author(s): Kang Shen

Last updated by author(s): Jun 6, 2024

Reporting Summary

Nature Portfolio wishes to improve the reproducibility of the work that we publish. This form provides structure for consistency and transparency in reporting. For further information on Nature Portfolio policies, see our Editorial Policies and the Editorial Policy Checklist.

Statistics

For all statistical analyses, confirm that the following items are present in the figure legend, table legend, main text, or Methods section.

n/a	Confirmed	
☐	☒	The exact sample size (n) for each experimental group/condition, given as a discrete number and unit of measurement
☐	☒	A statement on whether measurements were taken from distinct samples or whether the same sample was measured repeatedly
☐	☒	The statistical test(s) used AND whether they are one- or two-sided *Only common tests should be described solely by name; describe more complex techniques in the Methods section.*
☒	☐	A description of all covariates tested
☐	☒	A description of any assumptions or corrections, such as tests of normality and adjustment for multiple comparisons
☐	☒	A full description of the statistical parameters including central tendency (e.g. means) or other basic estimates (e.g. regression coefficient) AND variation (e.g. standard deviation) or associated estimates of uncertainty (e.g. confidence intervals)
☐	☒	For null hypothesis testing, the test statistic (e.g. F, t, r) with confidence intervals, effect sizes, degrees of freedom and P value noted *Give P values as exact values whenever suitable.*
☒	☐	For Bayesian analysis, information on the choice of priors and Markov chain Monte Carlo settings
☒	☐	For hierarchical and complex designs, identification of the appropriate level for tests and full reporting of outcomes
☒	☐	Estimates of effect sizes (e.g. Cohen's d, Pearson's r), indicating how they were calculated

Our web collection on statistics for biologists contains articles on many of the points above.

Software and code

Policy information about availability of computer code

Data collection	3i Slidebook (v6) was used to collect all microscopy images.
Data analysis	Images were analyzed using Fiji (v.2.1), statistics were performed using GraphPad Prism (v.9) or Excel (v.16.69.1). Bioinformatics was performed using R (v.4.1.1), drawProteins (v.3.16), HOMER (v.4.11), Damidseq_pipeline (v.1.5.3), find_peaks (v.1.0.1), FastQC (v.0.11.9), Bowtie2 (v.2.5.1), Samtools (v.1.14), Seqplots (v.3.0.12), atac-seq-pipeline (v.1.14), bedtools (v.2.28), Gene Ontology Database (PANTHER overrepresentation test (release: 2022-10-07) with the GO Ontology database (release 2022-07-01).

For manuscripts utilizing custom algorithms or software that are central to the research but not yet described in published literature, software must be made available to editors and reviewers. We strongly encourage code deposition in a community repository (e.g. GitHub). See the Nature Portfolio guidelines for submitting code & software for further information.

Data

Policy information about availability of data

All manuscripts must include a data availability statement. This statement should provide the following information, where applicable:

- Accession codes, unique identifiers, or web links for publicly available datasets
- A description of any restrictions on data availability
- For clinical datasets or third party data, please ensure that the statement adheres to our policy

All sequencing data generated in this study is publicly available in Gene Expression Omnibus GEO: GSE260637. Data has been released.

Research involving human participants, their data, or biological material

Policy information about studies with [human participants or human data](). See also policy information about [sex, gender (identity/presentation), and sexual orientation]() and [race, ethnicity and racism]().

Reporting on sex and gender	N/A
Reporting on race, ethnicity, or other socially relevant groupings	N/A
Population characteristics	N/A
Recruitment	N/A
Ethics oversight	N/A

Note that full information on the approval of the study protocol must also be provided in the manuscript.

Field-specific reporting

Please select the one below that is the best fit for your research. If you are not sure, read the appropriate sections before making your selection.

☒ Life sciences   ☐ Behavioural & social sciences   ☐ Ecological, evolutionary & environmental sciences

For a reference copy of the document with all sections, see nature.com/documents/nr-reporting-summary-flat.pdf

Life sciences study design

All studies must disclose on these points even when the disclosure is negative.

Sample size	No power analyses were used to determine the sample size of animals used for the study. Appropriate sample sizes were based on published literature in the field. 10-20 animals/cells were used for each condition as used previously in PMIDs:30146163; 35259341. Specific sample sizes are reported in the figure legends. For measurements of worm synapses and nuclei, each dot represents an individual cell or animal. For qPCR experiments, each dot represents an independent biological replicate.
Data exclusions	No data were excluded.
Replication	Biological replicates were defined as distinct C. elegans animals. All C. elegans in vivo microscopy measurements were performed and repeated in at least two indepedent imaging sessions. All attempts at replication were successful. For qPCR experiments, for each primer set tested, 3 technical replicates were performed for each biological replicate (3 biological replicate). To reduce batch effects, for each experiment, all RNA was processed simultaneously, converted to cDNA and subjected to qPCR using master mixes. Behavioural experiments were repeated three times and all attempts at replication were successful.
Randomization	Randomization was not necessary for these experiments as they were performed based on genotype and treatment.
Blinding	Experimenters were blinded to the genotype of animals for all behavioural experiments. For imaging experiments, experimenters were not blinded since mutant/treatment phenotypes were easily observable and could not be effectively blinded.

Reporting for specific materials, systems and methods

We require information from authors about some types of materials, experimental systems and methods used in many studies. Here, indicate whether each material, system or method listed is relevant to your study. If you are not sure if a list item applies to your research, read the appropriate section before selecting a response.

Materials & experimental systems

n/a	Involved in the study
☐	☒ Antibodies
☒	☐ Eukaryotic cell lines
☒	☐ Palaeontology and archaeology
☐	☒ Animals and other organisms
☒	☐ Clinical data
☒	☐ Dual use research of concern
☒	☐ Plants

Methods

n/a	Involved in the study
☒	☐ ChIP-seq
☐	☒ Flow cytometry
☒	☐ MRI-based neuroimaging

Antibodies

Antibodies used	Chromotek GFP TRAP (GFP Nanobody/ VHH coupled to agarose beads, cat#: gta)
Validation	Antibodies used were standard commercial antibodies and were validated by the manufacturer. No custom antibodies were used.

Animals and other research organisms

Policy information about studies involving animals; ARRIVE guidelines recommended for reporting animal research, and Sex and Gender in Research

Laboratory animals	Bristol N2 C. elegans animals were used for all experiments. Animals used in this study were all hermaphrodites and were between the developmental ages of L2 and L4. Complete strain list is provided in Supplementary Table 13. Specific ages of animals used in each experiment are listed in the Methods and in the Figure Legends.
Wild animals	No wild animals or isolates were used.
Reporting on sex	All animals used for imaging were hermaphrodites; male animals were solely used for genetic crosses.
Field-collected samples	No field-collected samples were used.
Ethics oversight	C. elegans are invertebrates and thus did not require any ethical approvals to conduct these experiments. No controlled compounds were used in this study.

Note that full information on the approval of the study protocol must also be provided in the manuscript.

Flow Cytometry

Plots

Confirm that:

☒ The axis labels state the marker and fluorochrome used (e.g. CD4-FITC).

☒ The axis scales are clearly visible. Include numbers along axes only for bottom left plot of group (a 'group' is an analysis of identical markers).

☒ All plots are contour plots with outliers or pseudocolor plots.

☒ A numerical value for number of cells or percentage (with statistics) is provided.

Methodology

Sample preparation	Described in Materials and Methods. Briefly, worm nuclei was obtained by douncing in a stainless steel dounce. Nuclei was separated by centrifugation and filtered through a 5um filter. Nuclei were stained using DAPI (ThermoFisher) according to manufacturer protocols.
Instrument	BD FACS Aria Fusion
Software	BD FACSDiva
Cell population abundance	2.3% of events were selected for based on gating strategy (See Figure S5). Samples were assessed for purity by reanalyzing post-sort samples. Samples with over 95% purity were processed for ATAC-seq.
Gating strategy	Gating strategy is as shown in Supplementary Figure 12 and was established based on experience by staff at the Stanford Shared FACS core. Preliminary FSC/SSC gating was drawn to select against debris (larger than 10^2 SSC-A signal and larger than ~10^3 FSC-A signal). Our nuclei isolation protocol results in many debris despite sucrose washes. During our optimization, we placed gates over the 'debris' region and placed a drop of the sorted particles on a slide to verify the presence or absence of nuclei. GFP gates were drawn using animals that do not express GFP, and similarly, positive and negative gates were confirmed by visualizing sorted particles on a microscope to confirm stringency/efficiency of gating.

☒ Tick this box to confirm that a figure exemplifying the gating strategy is provided in the Supplementary Information.